*remote sensing*

MDPI

*Article*

# Modeling the Spectral Properties of Obtrusive Light Incident on a Window: Application to Montréal, Canada

**Martin Aubé [1,2,3,*], Julien-Pierre Houle [1], Justine Desmarais [1], Nikki Veilleux [1] and Émie Bordeleau [1]**

[1] Department of Physics, Cégep de Sherbrooke, Sherbrooke, QC J1E 4K1, Canada; julien-pierre.houle@umontreal.ca (J.-P.H.); Justine.Desmarais@USherbrooke.ca (J.D.); nikkiveilleux@outlook.com (N.V.); emie.bordeleau@usherbrooke.ca (É.B.)
[2] Département de Géomatique Appliquée, Université de Sherbrooke, Sherbrooke, QC J1H 2R1, Canada
[3] Physics Department, Bishop's University, Sherbrooke, QC J1M 1Z7, Canada
* Correspondence: martin.aube@cegepsherbrooke.qc.ca; Tel.: +1-819-564-6350 (ext. 4146)

**Abstract:** This paper describes the use of a new obtrusive light module of the Illumina v2 model to estimate the light that may enter bedroom windows. We used the following as input to the model: (1) the sources' flux and spectrum derived from the color images taken by astronauts from the International Space Station (ISS), (2) an association between source spectrum and angular emission, and (3) a per zone inventory of obstacles properties and lamp height. The model calculates the spectral irradiance incident to buildings' windows taking into account the orientation of the street. By using the color information from an ISS image, we can classify pixels as a function of their spectra. With the same image, it is also possible to determine the upward photopic radiance for each pixel. Both serve as inputs to the model to calculate the spectral irradiance on any window. By having the spectral irradiance, it is possible to determine the Melatonin Suppression Index and the photopic irradiance on the window. Such information can later be used to perform epidemiological studies. The new methodology is applied to the city of Montréal in Canada for a set of houses' locations. The computations are made for 2013 (pre-LED era).

**Keywords:** human health; light pollution; modeling; street light; Montréal; melatonin suppression; obtrusive light



**Citation:** Aubé, M.; Houle, J.-P.; Desmarais, J.; Veilleux, N.; Bordeleau, É. Modeling the Spectral Properties of Obtrusive Light Incident on a Window: Application to Montréal, Canada. *Remote Sens.* **2021**, *13*, 2767. https://doi.org/10.3390/rs13142767

Academic Editor: Yuyu Zhou

Received: 11 June 2021
Accepted: 10 July 2021
Published: 14 July 2021



## 1. Introduction

Innovations in the field of lighting have shaped the history of the last century. Due to their numerous uses, our society has become light-dependent. As any other innovation, lighting technologies come with their advantages and disadvantages. The negative aspects of these technologies seem to be unknown by most people. The unexpected effects of what is now called Artificial Light At Night (ALAN) have first been mentioned by astronomers. Within the past decade, multidisciplinary researchers became aware of the actual issues. Indeed, abnormal behaviors have been observed among several nocturnal species [1] due to ALAN. Negative impacts on bats [2], turtles [3], fish [4], and songbirds [5] have already been identified. Moreover, it is now known that ALAN has an effect on plants [6–10]. On the other hand, what seems even more concerning is the possible impacts of ALAN on human health. For humans, the first suspected impacts are related to breast and prostate cancers [11–13]. ALAN plays a role in disturbing circadian rhythm [14], even in low intensity lighting [15]. The disturbance to the circadian cycle also plays a role in the increase of obesity [16]. In order to provide a reference to establish the potential impact of a given spectrum of ALAN on the melatonin suppression, Aubé et al., 2013 [17] introduced the Melatonin Suppression Index (MSI). The MSI is a dimensionless indicator. It is calculated by taking the ratio of the integral of the constant lumen spectrum of the target light multiplied with the melatonin suppression action spectrum over the same integral but replacing the target light spectrum by the constant lumen standard illuminant D65

spectrum. The MSI is therefore independent of the lamp flux. The MSI only tells us how a spectrum shape fits the melatonin suppression action spectrum compared to the way the D65 illuminant does. At its introduction, some studies verified if associations exist between the MSI and a variety of diseases. Among them, the authors of Garcia-Saenz et al. [18,19] found that, for Spanish cities, regions with high MSI are associated with increased risk of breast, prostate, and colorectal cancers.

The goal of this paper is to present a new methodology combining color remote sensing of the lighting technologies with a radiative transfer model to determine the spectral irradiance falling on a window facing a street at any location. We will show how such a method can provide new information compared to using spaceborne images solely. The method is firstly applied to the Montréal's lighting infrastructure as it was in 2013, before the massive street light conversion to Light-Emitting Diodes (LED).

## 2. Modeling Approaches

Over the past decades, models have been designed in order to reach a common goal: modeling the sky brightness for a given area. The first numerical model has been designed by R.H. Garstang in the 1980s [20]. Compared to the most recent models, it was relatively simplistic. In fact, the angular light output pattern (LOP) was prescribed and needed to be uniform everywhere. Furthermore, the cities were circular with constant lumen per square kilometer, and had no topography. The main advantage of the Garstang model was based on its simplicity, speedy calculations, and on the ease of producing model inputs. Later on, the authors of Luginbuhl et al. [21], Cinzano and Falchi [22] improved the Garstang's model by allowing each pixel to be considered as a circular lighted surface. By combining a certain number of pixels, they could consider cities of any shapes. Different LOPs were suggested, some including a correction to mimic the screening effects of obstacles such as trees and buildings. More advanced models were proposed by the authors of Aubé et al. [23], Kocifaj [24]. These authors applied the resolution of the radiative transfer in more complex environments. The Illumina v0 model [23] makes it possible to include subgrid obstacles, variable aerosols, and a pixel-based light source inventory with variable spectra and LOP. From the beginning, Illumina incorporates the 2nd order of scattering. Illumina is extremely heavy and ideally requires access to a supercomputer [25]. Illumina was significantly upgraded in 2018 [26] and 2021 [27] by including a full hyperspectral support, improved subgrid obstacle blocking, improved resolution (tested down to 20 m), multiple aerosol layers including fog and dust, overhead clouds, and the calculation of the direct radiance and irradiance (from sources and reflecting surfaces). The latest available version is v2 [28].

All the above-mentioned models were initially designed with the aim of characterizing the impact of light pollution on the star visibility for astronomical purposes. When it comes to estimate the effect of light pollution on human health, one must first consider that the most affected areas are likely concentrated inside cities. Unlike what happens in the countryside, the light pollution field in cities is clearly dominated by the light coming directly from the lighting devices without interfering significantly with the atmosphere. That light may enter buildings' and houses' windows directly and after reflection on nearby surfaces. To allow the estimation of the obtrusive direct light, a new module has been added to the Illumina in its version v2. The Illumina v2 model throws a set of photons from each individual light source and then reaches the observer's field of view. The model considers six different paths borrowed by the photons. Those include two single scattering, two second-order scattering, and two direct light paths. When it is time to determine the obtrusive light in a city, the last two paths are the most significant. There are many modeling parameters defined independently for each grid cell such as the radiant spectral flux, the LOPs, the ground reflectance, the ground altitude, the lamp's height relative to the ground, and the subgrid obstacle characteristics [26,27,29,30]. According to this set of input data, the spectral and angular characteristics of the lamps' infrastructure can be defined in the model. Used jointly with the orientation of the nearby street, one can determine the

amount of light falling on the surface of a window if we assume a window facing the street on a vertical facade parallel to the street. That amount of light is dominated by two main paths: (1) the direct path from the light fixture and (2) the light coming after the diffuse reflection on the ground or even buildings (when using resolution of the order of a meter or better). For a typical summer ground reflectance, the obtrusive light on the window that is coming after reflection on the ground is of the order of 1/10th of the obtrusive light coming directly from the light sources, while the obtrusive light coming back to the window after reflection on the opposite buildings' facades represents only as little as 1/100th of the obtrusive direct light. For that reason, we do not need to use very high resolution as a way to account for reflection on buildings. However, when the ground is covered with fresh snow, the reflection on the ground can rise up to the same order of magnitude as the obtrusive direct light.

## 3. Modeling Domain and Period

Throughout this modeling experiment, we used a resolution of 8.5 m which is approximately the resolution of the ISS image used to determine the lamp inventory. For that experiment, we consider the position of each house's window where we want to find the obtrusive light as a new virtual observer. Illumina v2 considers each virtual observer as a different model run and always locates the virtual observer in the center of the modeling domain. In this experiment, we used two layers having a size of 25 × 25 pixels. The first layer is a square of 212.5 × 212.5 m at a resolution of 8.5 m centered on the virtual observer. The second layer has a resolution of 21.25 m (531.25 × 531.25 m). The second layer excludes the first layer extent, meaning that the 21.25 m resolution only applies to sources located outside the central square of 212.5 m × 212.5 m defined by the first layer. This is large enough because we do not want to calculate the contribution of the light scattered by the sky that is considered negligible. One advantage of such a configuration is the rapidity of execution of Illumina v2.

Montréal is the second-biggest city in Canada, with 1,704,694 citizens in 2016 [31]. The city has a population density of 4662.1 citizens per square kilometer [31]. Overall, the city has a surface of 365.65 square kilometers [31]. As for the topography, it is relatively flat, except for a small hill named Mont Royal. The city contains more than forty skyscrapers higher than one hundred meters [32] and the overall building density is high. It is also common to see trees positioned near street lamps, blocking a part of the emitted light during summer.

Before the massive conversion to LED starting in 2017, Montréal has a street lighting mainly composed of High-Pressure Sodium (HPS) and Metal Halide (MH) lamps. The street lights photometry of HPS was mainly assimilated to a ≈50–50 mix of cobrahead-like and helios-like light fixtures with, respectively, ≈5% and ≈1% of the Upward Light Output Ratio (ULOR). Such a mix results in a 2% ULOR on average. Most MH lamps were cobrahead-like ≈5% ULOR. Some private lights are assumed to be mainly composed of Compact Fluorescent lamps (CFL) with a 15% ULOR. This information is summarized in Table 1. The modeling experiment presented hereby only considers the light sources extracted from an ISS image (see Figure 1). This image covers a surface of about 850 $km^2$. All sources falling outside this surface are not considered in our modeling experiment. This is not a problem as we are concerned about the obtrusive light coming from inside a radius of a few hundreds of meters. If one is concerned about the obtrusive light coming from the sky, Simoneau et al. [33] showed that about 90% comes from within 10 km but that situation is not considered in this study.

**Table 1.** Light fixtures characteristics per spectral class. The Correlated Color Temperature (CCT) and MSI are also given for each spectrum.

| Class | Technology | ULOR | LOP | CCT | MSI |
|---|---|---|---|---|---|
| | | % | | K | |
| 1 | Metal Halide | 5 | Cobrahead | 4700 | 0.58 |
| 2 | Metal Halide | 5 | Cobrahead | 3200 | 0.44 |
| 3 | Compact Fluorescent Lamp | 15 | Farm lantern | 3000 | 0.26 |
| 4 | High-Pressure Sodium | 2 | 0.5 cobrahead + 0.5 helios | 1940 | 0.08 |
| 5 | High-Pressure Sodium | 2 | 0.5 cobrahead + 0.5 helios | 2010 | 0.12 |
| 6 | Low-Pressure Sodium | 0 | Helios | 1750 | 0.02 |

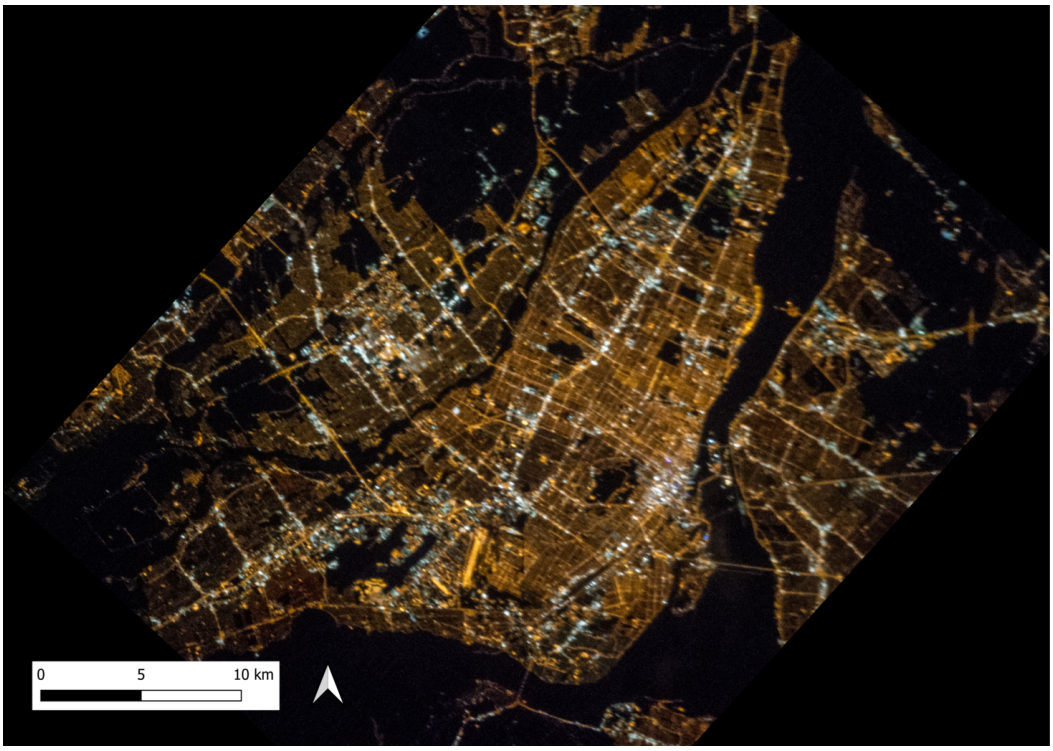


**Figure 1.** Georeferenced image of Montréal from the ISS taken on 6 April 2013.

## 4. Modeling Parameters

In order to achieve the modeling, a few parameters need to be determined. Those parameters are used as the base information for the model to be executed. We chose year 2013 as a reference period for the pre-conversion to LED lighting. The datasets can be divided into two main types: the uniform parameters and the gridded parameters. Those last ones are the parameters that may vary throughout the modeling domain.

### *4.1. Uniform Parameters*

Many of the uniform parameters are related to the atmosphere. However, as we are focusing on the obtrusive light, the atmosphere do not transform significantly the calculated values especially because that the distances between the light fixtures and the windows are small. Nevertheless, Illumina v2 require these parameters to be defined.

The first parameter used in the model is the relative humidity. The relevance of this parameter is related to the fact that many aerosols are hydrophilic and consequently their properties, such as their size and their refractive index, are influenced by it. To determine the value that we used for the modeling, we took the average humidity that has been recorded during early 2010s for Montréal City, which is approximately 79.1%, and rounded it to 80% [34].

Using the same methodology as above, the average atmospheric pressure for Montréal City has been set for the model as 101.1 kPa [34]. This parameter has an influence over the density of molecules present in the modeling domain, thus affecting their interactions with photons.

Other parameters considered to be uniform over the whole domain are the aerosol optical depth and the Ångström coefficient which are linked to the aerosol density and the size distribution. For this modeling experiment, we used the data available on the aerosol robotic network (AERONET) website [35]. More precisely, the data used, both for the Ångström coefficient and the aerosol optical depth (AOD), is the level 2 daily average values recorded on April 8, 2013 at the closest AERONET site (CARTEL). AOD average values are indexed according to the wavelength. We selected the AOD relative to a wavelength of 500 nm, while the Ångström coefficient is the one recorded for wavelengths 440 nm and 870 nm. A primordial parameter is the ground reflectance. We assumed a mix of 90% asphalt and 10% vegetation to be representative. Table 2 shows the values of each uniform all over the domain parameter used for the modeling.

**Table 2.** Uniform all over the domain input parameters used for the modeling. All parameters are required by Illumina v2 but the last column indicate the importance of the parameter for obtrusive light calculations. The urban aerosol model refers to the aerosol composition and size distributions defined by [36].

| Parameter | Value(s) | Units | Influence |
|---|---|---|---|
| Relative humidity | 80.0 | % | low |
| Atmospheric pressure | 101.1 | kPa | low |
| Aerosol optical depth | 0.15 | - | low |
| Ångström coefficient | 1.52 | - | low |
| Aerosol model | urban | - | low |
| Aerosol profile scale height | 2 | km | low |
| Clouds | None | - | low |
| Additional particle layer | None | - | low |
| Surface reflectance | 10% grass & 90% asphalt | % | high |
| Wavelength bins | 10 | | moderate |
| Wavelength bins width | 50 | nm | moderate |
| Starting wavelength | 350 | nm | moderate |

### *4.2. Gridded Parameters*

The first nonuniform parameter over the whole domain that is required is the digital elevation model (DEM). This parameter, which is basically the topography of the modeling domain, is obtained from the Shuttle Radar Topography Mission (SRTM) [37]. The absolute accuracy concerning the vertical altitude is of 16 m, while the accuracy of the relative height between two ground elements is of 10 m. The horizontal resolution is about 30 m.

### *4.3. Lamp Flux and Spectral Type from ISS Images*

The upward ISS photopic radiance and the lamp spectrum classification come from the ISS night images [38]. We used the ISS035-E-17088 image taken during the ISS035 mission with the Nikon D3S Camera (400 mm lens) on 6 April 2013 (Figure 1). We used preprocessed images provided by NOKTOsat [39], from which we developed a filtering process to remove the natural background radiance and the noisy signal over unlit surfaces. This allowed to limit the number of light-emitting pixels to the significant ones. Figure 2 summarizes the steps undertaken in order to obtain filtered ISS images. The quality of ISS images vary greatly depending on the image used. Some images may be blurred or badly impacted by a too high nadir viewing angle. For this study, we selected the best available image for both of these factors. The image calibration followed the method described in [38]. Although it is not a perfect database, it is far better than using the Visible Infrared Imaging Radiometer Suite Day Night Band (VIIRS-DNB Elvidge et al. [40]) satellite images as it is normally done with Illumina v2. First, because of the better spatial resolution of 8.5 m for the ISS images selected vs 750 m for VIIRS-DNB; and secondly because that the

color information is available from ISS while VIIRS-DNB is panchromatic and insensible to the blue.

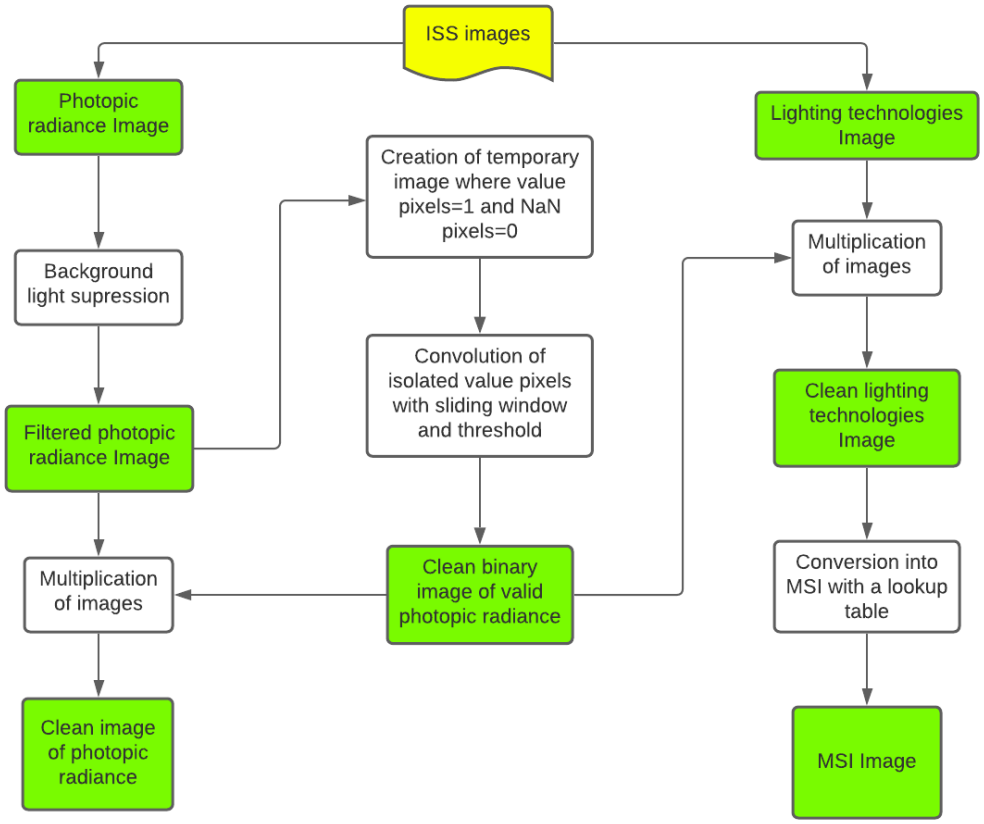


**Figure 2.** Organizational chart of steps undertaken to remove the background radiance and noise from the ISS images.

As a starting point, we had access to images conveying information on the photopic radiance (image ImpactVlG_GR from NOKTOsat) as well as the lighting technologies used throughout Montréal (image Composite from NOKTOsat). As for the second image, the technologies were separated into 5 different classes: number 1 relating to cool white sources (MH or LED higher than 4000 K); number 2 to warm white sources (CFL or MH between 3000 K and 4000 K); number 3 to a mix of 3000 K fluorescent, HPS, MH, or white sources between 2400 K and 3000 K; number 4 to phosphor converted (PC) Amber LED and warm HPS; and number 5 to normal HPS. A sixth category representing Low-Pressure Sodium (LPS) and pure amber LED is normally included in the image provided by NOKTOsat, but this category has not been detected in Montréal. There are very few pixels belonging to class number 3. Table 1 shows the choice of technology that we have made to meet the above classes in accordance to what was available in the city in 2013.

When looking at the photopic radiance image, it became apparent that there was some background lighting present in the image. This can be explained by the reflection of starlight, moonlight, and artificial sky glow on the surfaces along with the upward scattering of ground based lights. Indeed, the images revealed the presence of light in areas where there should not be anthropogenic light emitted at all (such as empty fields or bodies of water). In order to consider only artificial light emissions, we estimated the value of this background light and subtracted it from the value of every pixel in the image. This background was determined by a statistical analysis of the image. At first, a temporary image containing only the pixels of lesser value was created. As points of higher emission intensity had been eliminated, only light emissions in dark areas remained. We then analyzed this remaining data and estimated that the addition of the mode and the

standard deviation of this new image would be a good value for the background removal. Indeed, the background light is quite similar throughout the territory. It is therefore a logical assumption that the value of the background light is the most common value in the image. The standard deviation was also added to the background in order to completely eliminate the background light that could be somewhat higher than the mode in certain areas. The use of the standard deviation in the determination of the background was decided by trial and error. This empirical value fits well for the territory of study but might have to be changed when studying a different one with the same method.

Within this filtered image, isolated non-null pixels could still be found within areas that should not emit light. As to not consider these false light sources, this noise had to be eliminated from the data. A binary image was created in which the pixels were given a new value of 1 for non-null pixels and 0 for null pixels. A convolution was then applied to this binary image: a sliding window of 3 pixels by 3 pixels would consider the surrounding pixels of each individual pixel in order to determine if it needed to be eliminated. If a non-null pixel had 4 or more pixels of value 1 surrounding it (meaning that this pixel was not isolated within a dark area), it would remain of the value 1. If it had 3 or less pixels of value 1 in the sliding window, it would be given a new value of 0. This process resulted in a new binary image in which only the pixels that should realistically have a significant value were kept (the others having been converted to zeros). Finally, this binary image was multiplied to both the photopic radiance and the lighting technology images in order to obtain clean images (see Figures 3 and 4).

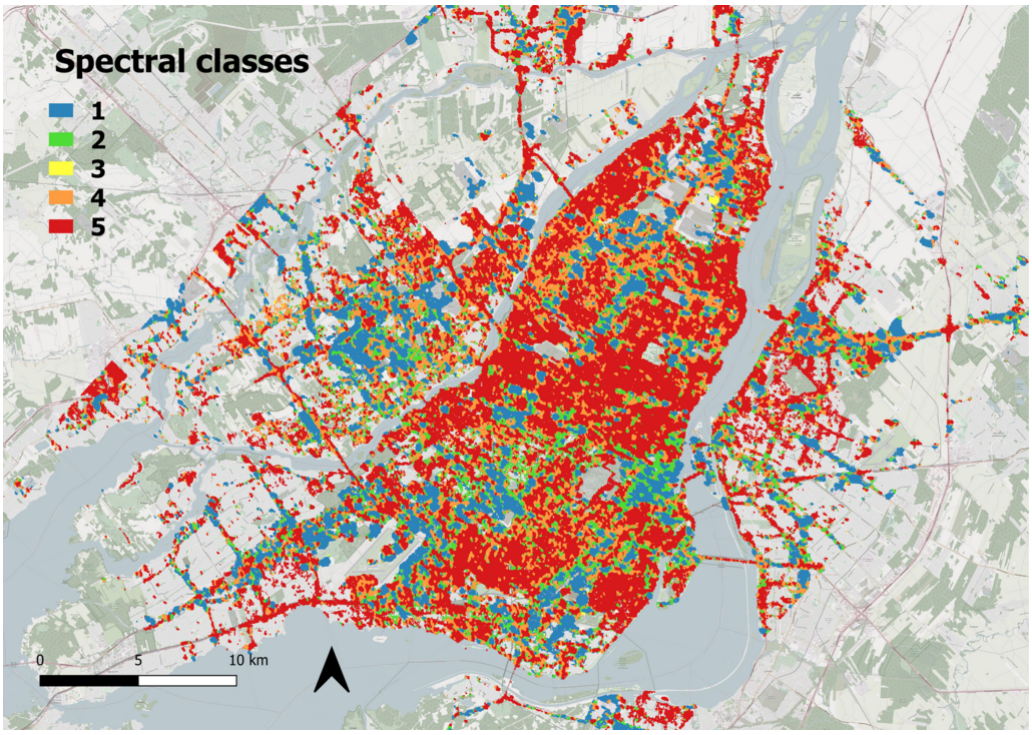


**Figure 3.** Filtered spectral classes image of Montréal from the ISS taken on 6 April 2013.

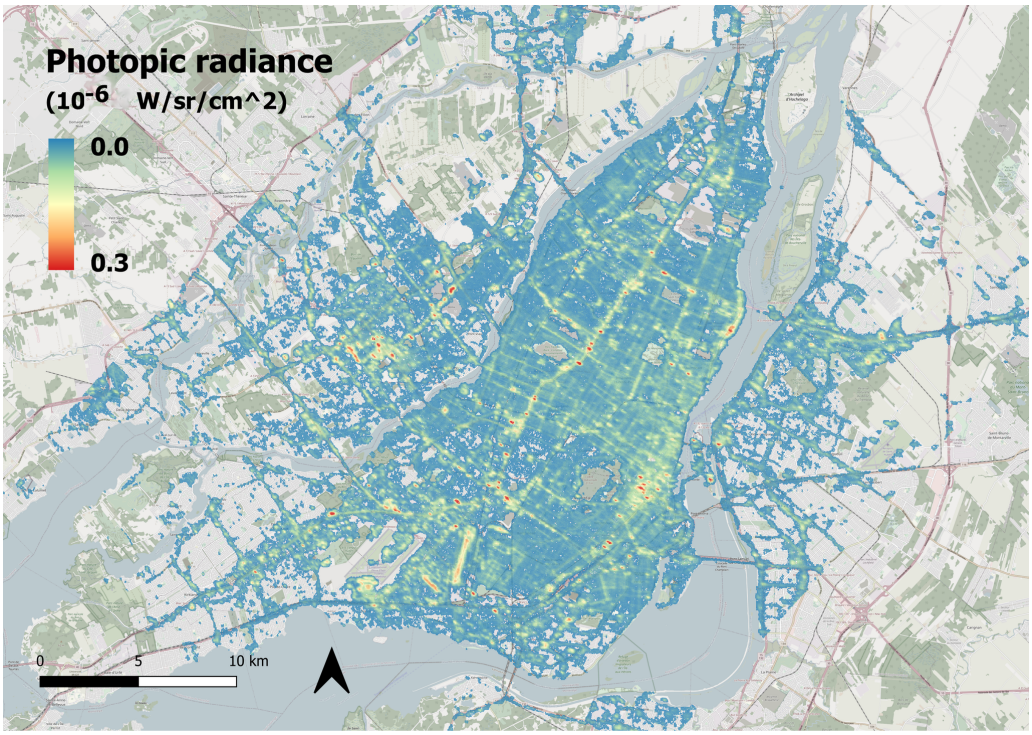


**Figure 4.** Filtered photopic radiance image of Montréal from the ISS taken on 6 April 2013.

Afterwards, we created an image of the MSI throughout Montréal from the information contained in the filtered lighting technology image (Figure 3). We estimated the MSI for each of the 5 categories of technology present in Montréal in 2013 (Table 1). We used the data on Lamp Spectral Power Distribution Database (LSPDD) [41] to find the relevant lamp and determined the associated MSI for each spectral class. We created a lookup table associating the MSI to its class. Finally, we substituted the value relating to the class for the value of the MSI in the image (Table 1). The resulting image therefore presents the MSI for each pixel. The MSI image is not shown because that it is almost identical to Figure 3, each class of Figure 3 being replaced by the relevant MSI value of Table 1.

### *4.4. Obstacle Properties and Lamps Heights*

The average height of street lamps and properties of the obstacles for each region are determined using Google Maps StreetView [42] and Google Earth [43]. A total of 309 circular zones with various radius and specific central coordinates have been defined with Map Developers [44] in order to cover the entire surface of Montréal. These zones were established according to the relative uniformity of the buildings' size, the distance between them, the lamps' height over the area, and the obstacle filling factor. The procedure established to collect the required information is the same for each zone. The circular zones are shown in Figure 5.

The first parameter defined for each zone is the average building height ($h_o$). This obstacle height was measured using the Path3D function in Google Earth. The average street lamp height ($h_L$) was also estimated for each zone using the same method. Then, the distance between the obstacles ($d_o$) (buildings, trees) was determined by using the ruler tool in Google Earth at an angle of $\sim 45^o$ from the street orientation. Although the closest obstacles would usually be in front or behind the street lamps, we considered that street lamps are engineered to direct light slightly in front of them but mostly in the direction of the street. Thus, we estimated that the average distance a photon could travel before colliding with an obstacle would be approximately equivalent to the distance of the first obstacle met at an angle of 45 degrees. We finally determined the obstacle filling factor ($F$). This obstacle property is a ratio out of one corresponding to the peripheral angle of a

position where the path of the photons is blocked. For instance, an obstacle filling factor of 0.5 is attributed to a position if ∼180° out of the total 360° are blocking light trespass.

Table A1 summarizes the various zones defined to characterize the obstacles and lamp heights. In Illumina, the order in which the zones are provided to the model is related to their priority (a new zone having a higher priority over the previous). In case of an intersection between zones, the latest zone overwrites the previous one. In Table A1, the zone number 1, established as the set of default values, is valid for regions where no other circular zone is defined (as any zone superimposed on the first predominates).

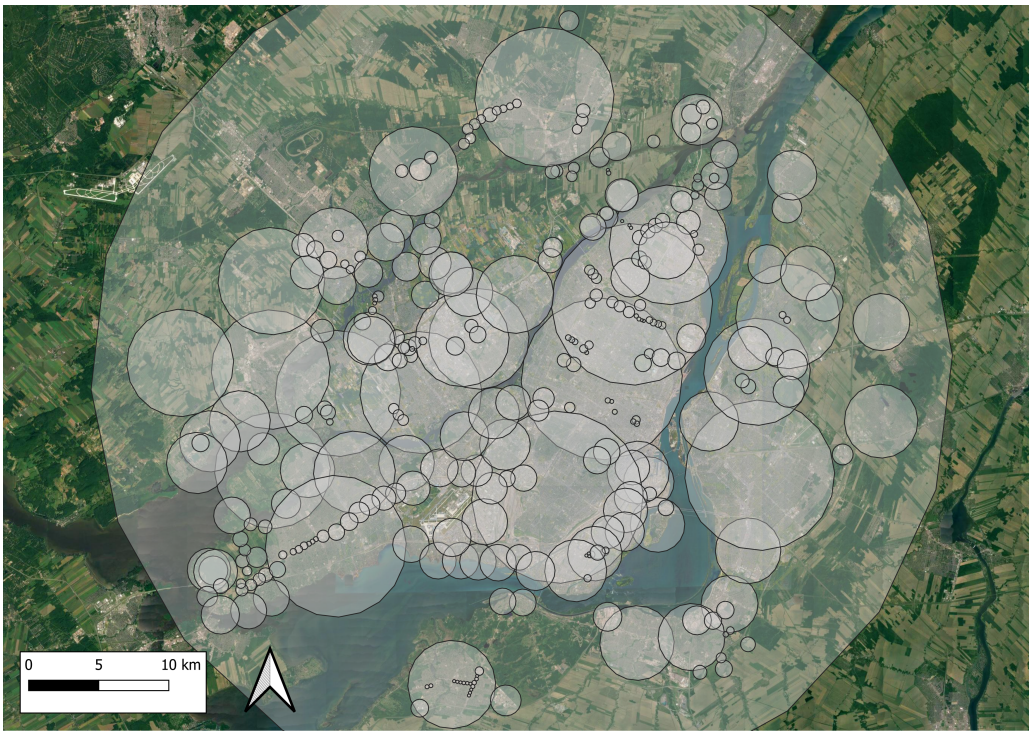


**Figure 5.** Map of the 309 zones established for the characterization of the lamps height and obstacles properties in Montréal. The complete characteristics of each zone is given in Table A1.

### *4.5. Generic Light Output Patterns and Spectra*

We considered 3 different ULORs: 2%, 5%, and 15%. The cobrahead-like LOP (5% ULOR) was taken from the Illuminating Engineering Society of North America (IESNA) file for the Cooper's cobrahead model. This LOP was systematically associated to MH lamps. The HPS LOPs are typically in relatively equal number of cobrahead (5% ULOR) and of Helios models (1% ULOR). The average of their IESNA files gives a new LOP with 2% ULOR. For the CFL, we assumed a LOP having 15% ULOR. In the latter case, the LOP was measured by ourselves with a farm lantern (model Globe PL-8120). To achieve that measurement we installed the farm lantern on a dual axis rotating system and measured the illuminance falling on a lux meter for a variety of angles. The lux meter was installed 4 m away from the lantern and the experiment was done in a black painted room to minimize the influence of the reflected light.

We used five different lamp spectra which were taken from the LSPDD. Figure 6 shows the spectra of the lamps used for this experiment. The associations between the spectra and the LOPs are given in Table 1.

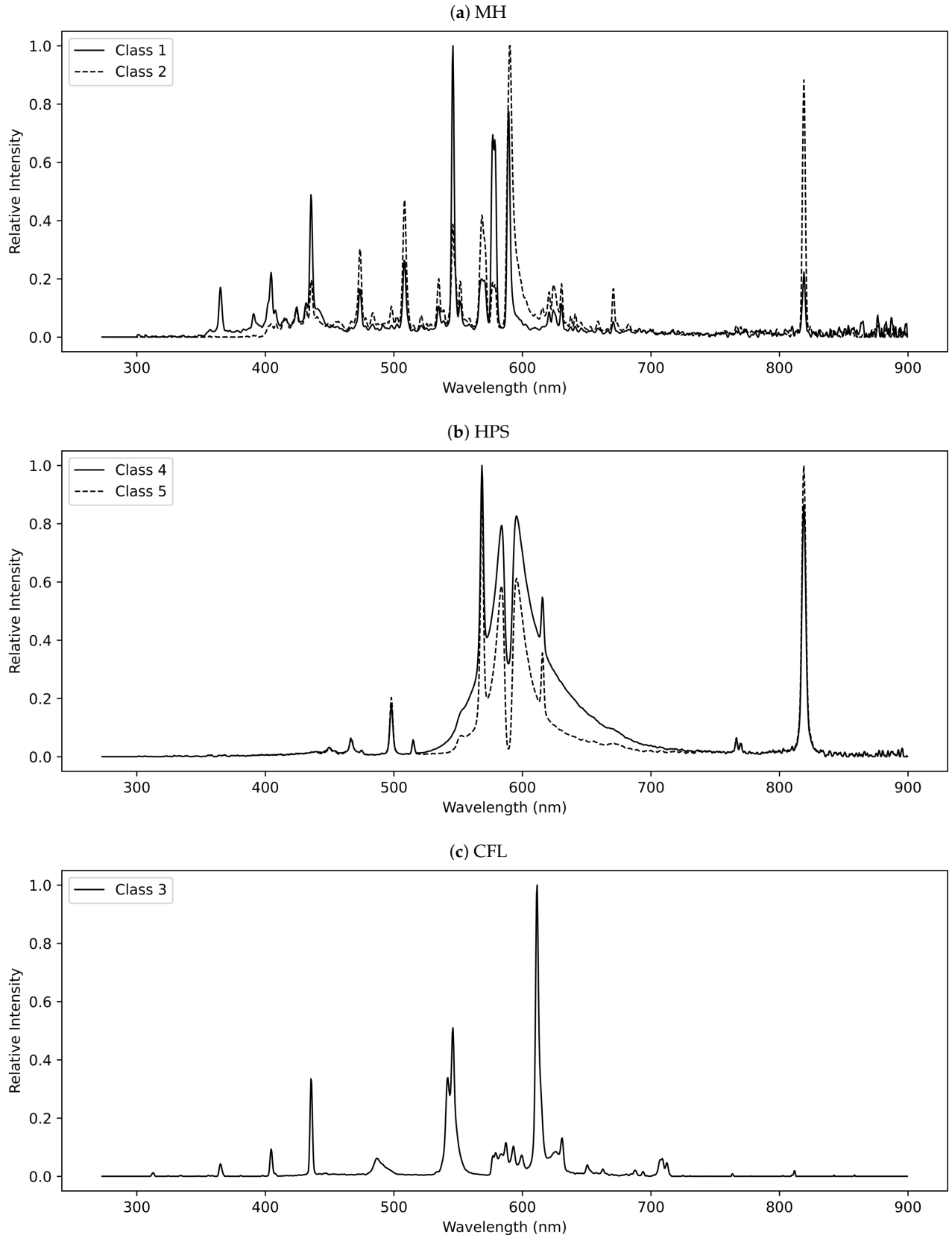


**Figure 6.** Spectra used for the modeling of Montréal in 2013. Panel (**a**) show the Metal Halides lamps spectra, panel (**b**) the High Pressure Sodium lamps spectra and panel (**c**) the Compact Fluorescent lamp spectrum.

For each pixel, we determine the spectrum and its radiant flux $\Phi_e$. This is done thanks to the ISS derived spectral classes and upward ISS photopic radiance images. Knowing the typical LOP and spectrum associated to each pixel according to its spectral class (see Table 1), one can convert the ISS-derived photopic radiance into spectral flux of the pixel (in Watt). This is done with Equation (1).

$$\Phi_e = \frac{L_{e,\Omega}(\theta) \times S}{\int_\lambda V(\lambda)T(\lambda)\left(\frac{1}{\pi}\rho(\lambda)F_{90-180}(\lambda) + \bar{G}(\theta,\lambda)\right)\mathrm{d}\lambda} \quad (1)$$

$L_{e,\Omega}(\theta)$ is the photopic radiance given by the ISS image Impact_VlG_GR (in units of nw sr$^{-1}$ cm$^{-2}$ Å$^{-1}$) multiplied by the nominal photopic bandwidth (∼1000 Å). $S$ is the area of the pixel in cm$^2$ (which is 722,500 cm$^2$ for a pixel of 8.5 m). $V(\lambda)$ is the spectral sensitivity of the photopic band. $\theta$ is the zenith angle between the image center and the ISS (31° in our case). $\rho(\lambda)$ is the ground reflectance. $F_{90-180}(\lambda)$ (see Equation (2)) and $\bar{G}(\theta,\lambda)$ are, respectively, the amount of light going down per unit of wavelength and the LOP value at any wavelength for the zenith angle $z = \theta$. In our application of the model to Montréal, $\bar{G}(\theta,\lambda)$ is given by the combination of the LOP and the spectrum for any given spectral class defined in Table 1. $T(\lambda)$ is the atmospheric transmittance but that factor has been already corrected by NOKTOsat so that we set its value to 1.

$$F_{90-180}(\lambda) = \int_{z=\frac{\pi}{2}}^{\pi} 2\pi \sin(z)\bar{G}(z,\lambda)\,\mathrm{d}z \quad (2)$$

According to the work in [26], the spectral intensity $I_{e,\Omega}(z,\lambda)$, in [W/sr/nm], leaving the light source pixel at any zenith angle $z$ is given by Equation (3).

$$I_{e,\Omega}(z,\lambda) = \bar{G}(z,\lambda)\Phi_e \quad (3)$$

The radiant flux of a pixel $\Phi_e$, in [W], is determined from the ISS photopic radiance image and Equation (1) combined with (1) information from the pixel net LOP and spectrum, (2) the photopic spectral response, and (3) the ground spectral reflectance [26]. $\bar{G}(z,\lambda)$, in [W sr$^{-1}$ nm$^{-1}$], is the light radiation pattern of a pixel. This function gives the relative amount of light emitted at any zenith angle and any wavelength per unit of solid angle. In Illumina's usual configuration, where we get the radiance from VIIRS-DNB, $\bar{G}(z,\lambda)$ of a given pixel is a combination of different street lamps having different LOPs and different spectra because of the large size of the pixel footprint. In the present adaptation to the higher-resolution data from ISS images, the LOP of a pixel is the same for any wavelength as we assume that only one light fixture falls inside a pixel (i.e., $\bar{G}(z,\lambda) = \bar{G}(z)$).

### *4.6. Determining the Window Orientation*

Determining the angle and orientation between the window and the street lamps is crucial to model the irradiance entering in a home. We assume a window facing the closest street so that the front of the house is parallel to the street. With the objective of making our modeling approach as general as possible, we developed a numerical method to determine, from any address in the world, the closest driving street. This is done by using OpenStreetMap data and an r-tree integrated in the OSMnx python library to calculate the minimal euclidean distances between points [45]. The library is also used as a tool to fragment into straight lines each small street segments. This allows obtaining the bearing angle of a segment even in curved streets. We then add the appropriate angle to get a right angle between the street and the window. This angle is then used as an input value to the Illumina model (the azimuth viewing angle). For the elevation viewing angles, we aim to determine the irradiance on the vertical surface of a window. Therefore, that the elevation angle is always equal to zero. Figure 7 shows the resulting angles for a small part of Montréal.

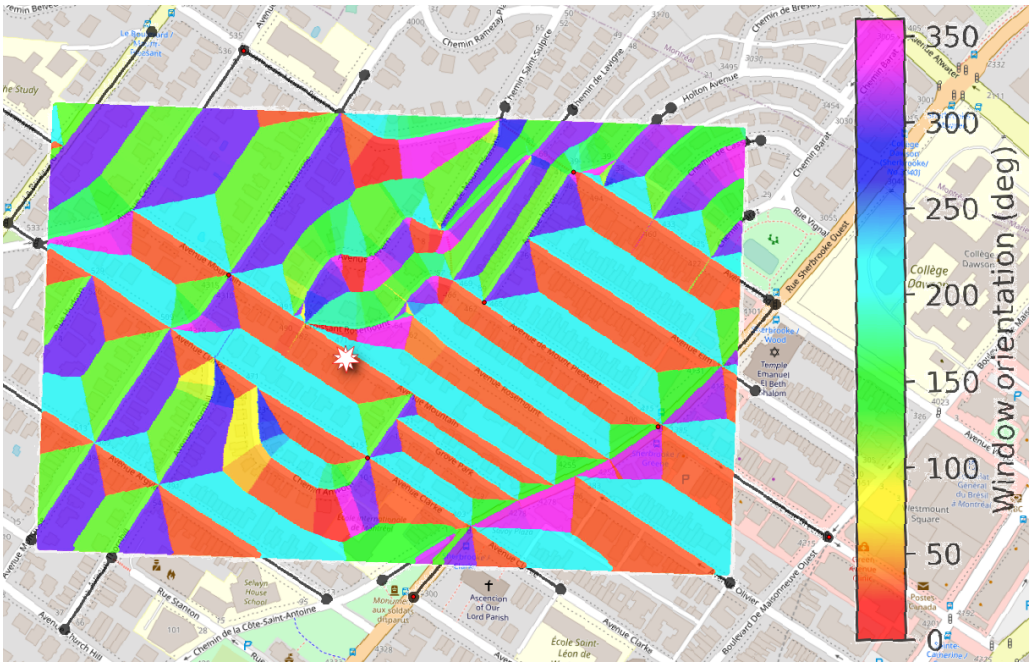


**Figure 7.** The azimuth angle of a window facing the nearest street derived from the street network. This figure is for a small part of Montréal centred on site #2 of Table 3. The white star marker indicates the position of site #2.

**Table 3.** List of modelled sites.

| # | Environment | Window Height | Latitude | Longitude | $d_o$ | $h_o$ | $F$ | $h_L$ |
|---|---|---|---|---|---|---|---|---|
| | | m | deg | deg | | | | |
| 1 | City center | 2, 5, 8 | 45.501171 | −73.565357 | 30 | 100 | 0.96 | 9 |
| 2 | Urban residential | 2, 5 | 45.488376 | −73.596217 | 37 | 12 | 0.93 | 8.5 |
| 3 | Suburb residential | 2 | 45.533026 | −73.703789 | 40 | 11 | 0.93 | 8 |
| 4 | Commercial | 2, 5, 8 | 45.468995 | −73.542072 | 55 | 9 | 0.89 | 9.5 |
| 5 | Rural | 2, 5 | 45.642133 | −73.662191 | 0 | 0 | 0 | 7.5 |

## 5. Results for Some Montréal Sites in 2013

In order to test and compare our modeling and remote sensing methodologies, we identified five different sites across the modeling domain. They are differing by their urban zoning categories. We actually selected a site in the city center, another in an urban residential area, one in a suburb residential area, plus one in a commercial area and finally another in a rural area. Each site differ by their distances between buildings and buildings' heights. All precise locations are on a building facade facing the street. We defined up to three floors but for some sites only one or two were kept with respect to the actual height of the buildings. We used 2, 5, 8 m above ground as the default set of heights. Detailed information about the sites is shown in Table 3.

Table 4 shows the comparative results obtained with the two methods to estimate both the MSI and the amount of photopic light for the five sites. One can notice that for MSI, no significant variation occur according to the window height (Illumina MSI). On the other hand, the Illumina photopic irradiance decreases with the window height. There is no obvious link between the Illumina MSI and the upward ISS MSI. This is because that the Illumina MSI is determined by the combined effect of the different lamp fixtures located nearby the virtual observer. The averaging weight function depend on the distance to the lamp fixture and on their spectral flux and LOP. The same observation arises with the comparison of upward ISS photopic radiance and the Illumina photopic irradiance.

In order to better explore if the ISS-derived parameters are somehow correlated to the equivalent parameters determined with Illumina v2, we decided to select 500 sampling

points across the city. The 500 points locations are shown in Figure 8. If no significant new information is provided by Illumina v2 compared to the one derived from the ISS images, we should observe a relatively good correlation between the values obtained directly from the ISS images and the Illumina v2-derived values. Figure 9 shows scatter plots between the ISS image-derived values and their equivalent from Illumina v2. The figures clearly show that the datasets are lowly correlated. That means that Illumina v2 provides significant new information compared to the ISS-derived parameters. This information is a complex combination of the effect of the positions, spectral power distribution, and LOP of nearby sources. For that reason, such modeling results can represent an advantage over direct remote sensing techniques when it comes to verify if there is any associations between the ALAN and health issues. Figure 9 also shows that the correlation coefficient between the ISS MSI and Illumina v2 do not significantly change according to the window height. This result is consistent with the fact that for our five sites, no significant changes were observed with various window height. One can notice that, for the MSI correlations, the density of points is higher around the 1:1 relationship and that Illumina generally predict higher MSI for low ISS MSI values and lower MSI for high ISS MSI values (see panels (a–c) of Figure 9). This is normal because the Illumina MSI does not only involve the pixel's lamp but also the nearby ones so that Illumina provides a complex averaging effect on the MSI. This averaging effect being a combination of the decrease of the radiance according to the distance to the source, of the zenith angle from the source to the virtual observer, on the LOP and of the spectral power distribution of the source. In regions dominated by low MSI sources, the presence of a few high MSI lamps will increase the MSI while for regions dominated by high MSI sources, the MSI will be lowered by the presence of a few low MSI sources nearby.

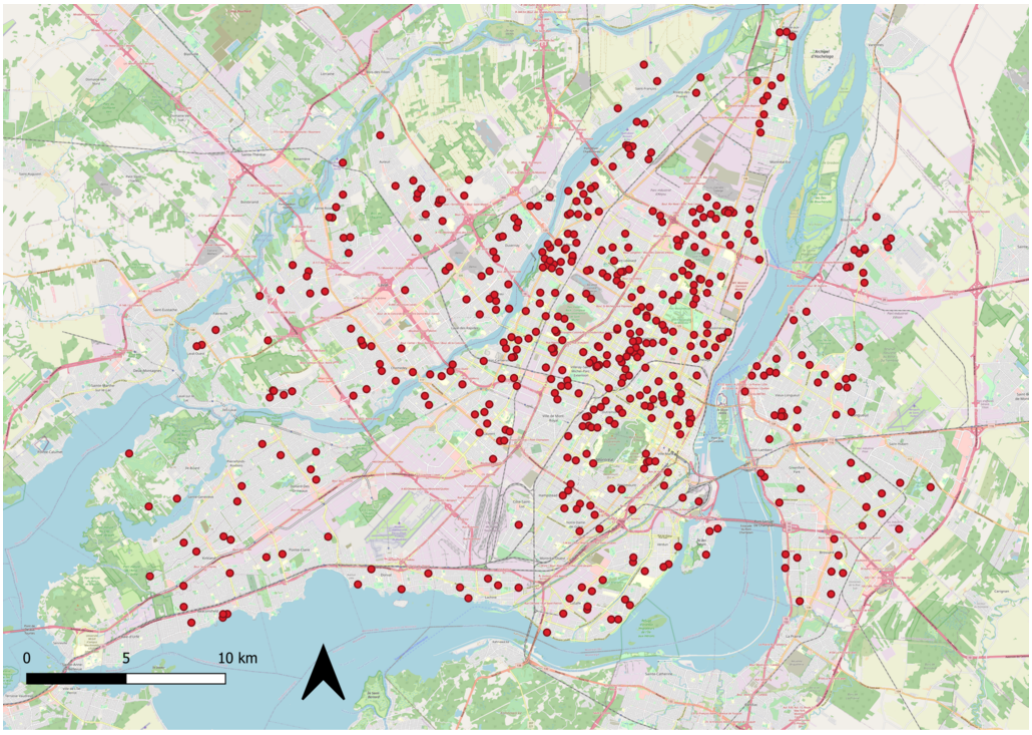


**Figure 8.** The location of the 500 sampling points across the city of Montréal.

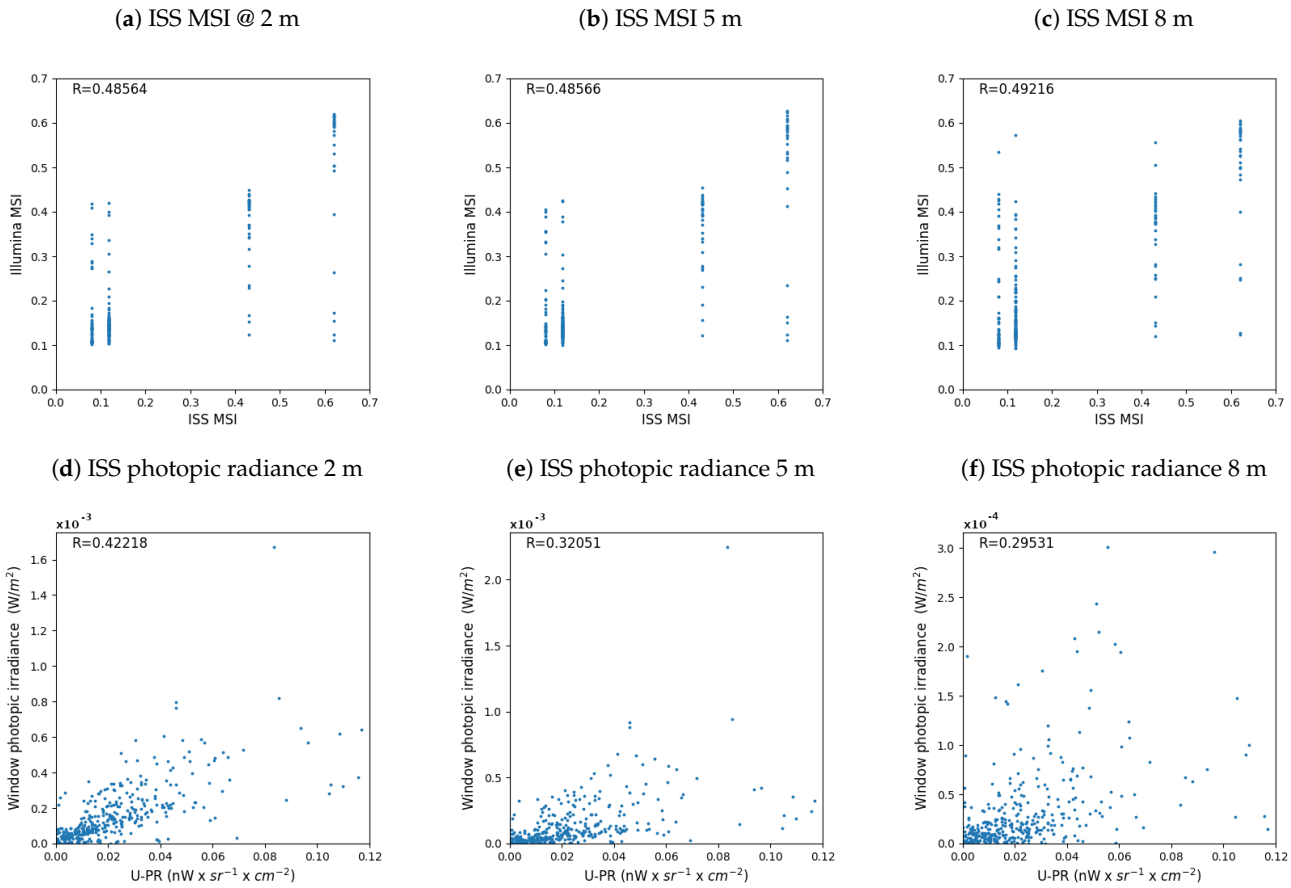


**Figure 9.** Scatter plots between the remotely sensed ISS MSI and MSI derived with Illumina v2 in panels (**a**–**c**), respectively, for window heights of 2, 5 and 8 m. Panels (**d**–**f**) show the scatter plots between the remotely sensed upward ISS photopic radiance and the Illumina photopic irradiance for the same set of window heights.

The relationship between the upward ISS photopic radiance and the Illumina photopic irradiance shows a decreasing correlation with higher window height. This may be because the radiance detected from space is dominated by the light reflected on the ground surface, and therefore we expect this light to be better correlated to the light going down or closer to the downward hemisphere.

Figure 10 shows the irradiance spectra obtained with Illumina v2 for the 5 sites for windows 2 m above ground. We only provided them for 2 m because almost no changes were observed in the spectra shapes with higher window height. The window height only influence significantly the level of light but not the spectral shape. For that reason, and given that the MSI is only sensitive to the spectrum shape, no significant change is observed with the MSI at different window height. It is also clear from Figure 10 that the spectrum is highly sensitive to the site location and the respective mix of lamp spectra located around each location. One nice aspect of using Illumina v2 is that it provides spectra. Having spectra allows a verification of any other lighting parameter, not only the MSI. As an example, one can calculate the CCT. Another interesting possibility provided by the model is to determine the photoreceptor response to the given irradiance by humans or any other animal specie. Illumina v2 also calculates the radiance spectra in a specific direction so that it can be useful when the direction of the light is of some importance. We did not use that feature in the present study.

(**a**) City center

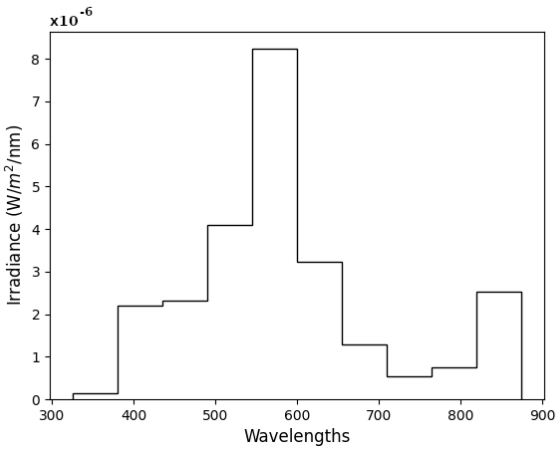


(**b**) Urban residential

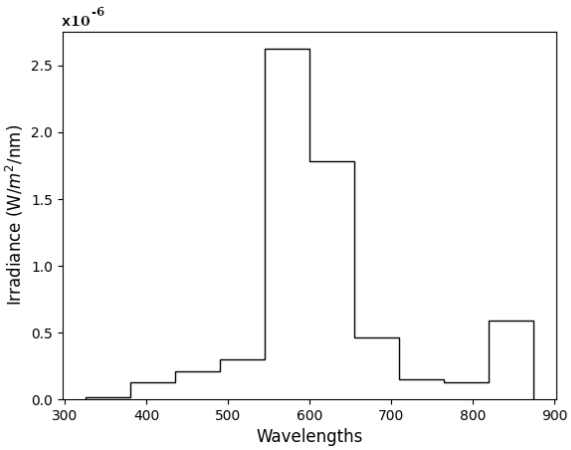


(**c**) Suburb residential

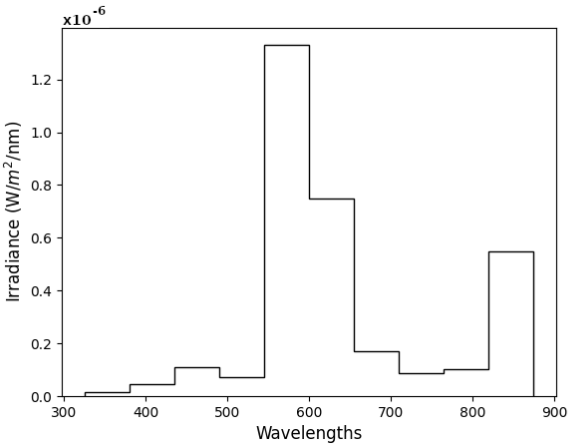


(**d**) Commercial

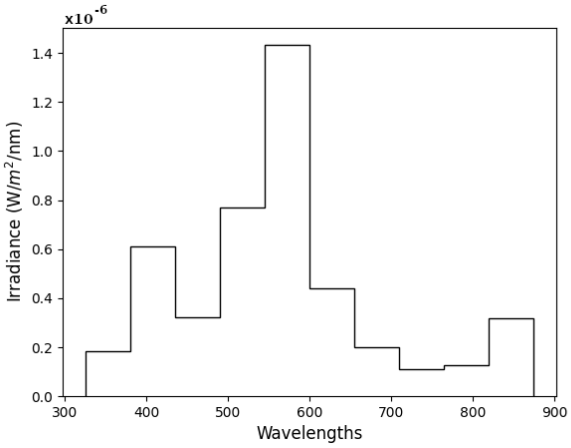


(**e**) Rural

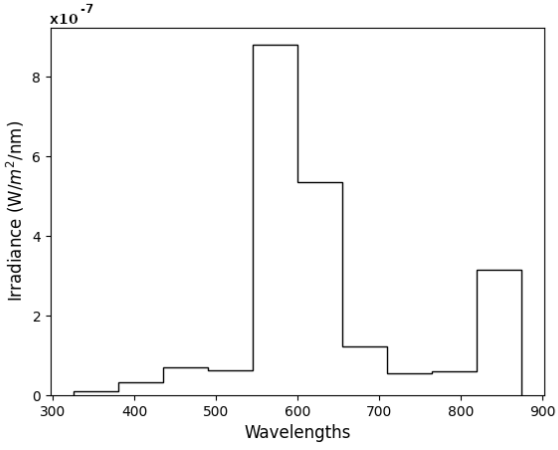


**Figure 10.** Spectral irradiance on windows 2 m above ground for the five test sites identified in Table 3. Panel (**a**–**e**) show respectively the spectral irradiance for the city center, the urban residential, the suburb residential, the commercial and the rural sites.

**Table 4.** Comparative results for the identified sites. Illumina MSI and Illumina photopic irradiance are the results obtained with Illumina v2, while ISS MSI and ISS photopic radiance are the values derived from the ISS images.

| # | Environment | Illumina Height | ISS MSI | Illumina MSI | ISS Photopic Radiance | Illumina Photopic Irradiance |
|---|---|---|---|---|---|---|
| | | m | | | $\mu W\ sr^{-1}\ cm^{-2}$ | $W\ m^{-2}$ |
| 1 | City center | 2 | 0.43 | 0.44 | 0.0442 | $5.91 \times 10^{-3}$ |
| | | 5 | | 0.44 | | $5.47 \times 10^{-3}$ |
| | | 8 | | 0.44 | | $3.18 \times 10^{-3}$ |
| 2 | Urban residential | 2 | 0.08 | 0.15 | 0.0135 | $1.59 \times 10^{-4}$ |
| | | 5 | | 0.14 | | $1.38 \times 10^{-4}$ |
| 3 | Suburb residential | 2 | 0.12 | 0.14 | 0.0128 | $7.51 \times 10^{-5}$ |
| 4 | Commercial | 2 | 0.62 | 0.53 | 0.0511 | $1.03 \times 10^{-4}$ |
| | | 5 | | 0.53 | | $9.52 \times 10^{-5}$ |
| | | 8 | | 0.53 | | $9.14 \times 10^{-5}$ |
| 5 | Rural | 2 | 0.12 | 0.14 | 0.0037 | $5.08 \times 10^{-5}$ |
| | | 5 | | 0.14 | | $2.17 \times 10^{-5}$ |

## 6. Conclusions

The goal of this paper was to present a new methodology combining color remote sensing of the lighting technologies with the radiative transfer model Illumina v2 to determine the spectral irradiance falling on a window surface facing a street at any location. By using the numerical model Illumina v2, we established that no clear correlation exists between the model results and the MSI and photopic radiances derived with the ISS images. The low correlation may indicate that Illumina v2 provides new information that is not available from the ISS images. We think that this result highlights that the use of Illumina v2 is promising to perform epidemiological studies related to the color and amount of obtrusive light. For that reason, we aim to provide such information to researchers in the field of epidemiology in order to verify if any association can be found between the Illumina v2 derived obtrusive light parameters and human health issues.

One other interesting result is that the Melatonin Suppression Index is almost insensitive to the window height, while the spectral irradiance decrease with the window height. Moreover, the correlation between the ISS-derived radiances and the Illumina v2 irradiances is worse for higher window heights. The reduction of the irradiance with height combined with the constant MSI is interesting to disentangle the effect of the spectral content versus the amount of light.

In the future, we plan to perform an in situ validation experiment in Montréal in order to determine the accuracy of the modeled approach presented here. That experiment will require the measurement of the irradiance on a set of sites for which we computed the Illumina v2 irradiance spectra. We are expecting to perform that experiment with the LANcube radiometer [46] in the coming year.

**Author Contributions:** We applied the sequence-determines-credit approach [47] for the sequence of authors which is in order of decreasing contributions. Conceptualization, M.A.; methodology, M.A., J.-P.H., J.D., N.V., and É.B.; software, M.A., J.-P.H., J.D., N.V., and É.B.; validation, M.A.; formal analysis, M.A.; investigation, M.A., J.-P.H., J.D., N.V., and É.B.; resources, M.A.; data curation, M.A.; writing—original draft preparation, M.A., J.-P.H., J.D., N.V., and É.B.; writing—review and editing, M.A., J.-P.H., J.D., N.V., and É.B.; visualization, M.A., J.-P.H., and J.D.; supervision, M.A.; project administration, M.A.; funding acquisition, M.A. All authors have read and agreed to the published version of the manuscript.

**Funding:** M.A. thanks the Fonds de recherche du Québec—Nature et technologies (FRQNT) for financial support through the Research program for college researchers. M.A. also thanks the Fonds de recherche du Québec—Santé for their financial support, M.A. and J.-P.H. thanks the Calcul Québec and Compute Canada for access to the Mammouth Parallel II supercomputer. M.A., J.-P.H.,

J.D., N.V., and É.B. thank Pôle régional en enseignement supérieur de l'Estrie (PRESE) for their financial support.

**Institutional Review Board Statement:** Not applicable.

**Informed Consent Statement:** Not applicable.

**Acknowledgments:** We thank Louis-Simon Babin, Carl Moreau, and Sandrine Hélie for their help with building part of the light inventory. We also thank Alexandre Simoneau for his support in adding new features to the Illumina input pipeline and for his help with the Python programming.

**Conflicts of Interest:** The authors declare no conflicts of interest.

## Appendix A. Montréal's Obstacle and Lamp Height Inventory

**Table A1.** Subgrid obstacles parameters and lamp heights used to model Montréal. The 309 zones were selected in order to define regions with relatively constant values.

| Zone | Latitude deg | Longitude deg | Radius m | $d_o$ m | $h_o$ m | $F$ | $h_L$ m |
|---|---|---|---|---|---|---|---|
| 1 | 45.557810 | −73.672506 | 30,650.92 | 0 | 0 | 0 | 7.5 |
| 2 | 45.494639 | −73.899268 | 4121.07 | 80 | 15 | 1 | 0 |
| 3 | 45.49488 | −73.867339 | 1948.43 | 35 | 11 | 0.93 | 4.5 |
| 4 | 45.508456 | −73.90757 | 1142.83 | 35 | 11 | 0.93 | 4.5 |
| 5 | 45.473517 | −73.886873 | 1048.83 | 35 | 11 | 0.93 | 4.5 |
| 6 | 45.543776 | −73.839687 | 4471.36 | 35 | 10 | 0.93 | 8.5 |
| 7 | 45.558958 | −73.90086 | 4233.07 | 35 | 10 | 0.93 | 8.5 |
| 8 | 45.526015 | −73.929013 | 2172.61 | 35 | 10 | 0.93 | 8.5 |
| 9 | 45.513235 | −73.956225 | 2172.61 | 35 | 10 | 0.93 | 8.5 |
| 10 | 45.499443 | −73.968007 | 2172.32 | 35 | 10 | 0.93 | 8.5 |
| 11 | 45.512158 | −73.964755 | 617.456 | 0 | 15 | 1 | 0 |
| 12 | 45.563189 | −73.983275 | 3804.76 | 0 | 0 | 0 | 7.5 |
| 13 | 45.615289 | −73.900191 | 3798.04 | 0 | 0 | 0 | 7.5 |
| 14 | 45.43119 | −73.957087 | 1550.37 | 43 | 11 | 0.93 | 8 |
| 15 | 45.430829 | −73.953139 | 1035.49 | 0 | 15 | 1 | 0 |
| 16 | 45.553076 | −73.599566 | 5734.21 | 40 | 11 | 0.93 | 8 |
| 17 | 45.600549 | −73.571945 | 5729.25 | 40 | 11 | 0.93 | 8 |
| 18 | 45.638371 | −73.538642 | 4233.28 | 40 | 11 | 0.93 | 8 |
| 19 | 45.487212 | −73.556747 | 1801.99 | 55 | 9 | 0.89 | 9.5 |
| 20 | 45.459964 | −73.548806 | 1943.82 | 45 | 13 | 0.97 | 8 |
| 21 | 45.470838 | −73.541125 | 559.52 | 55 | 9 | 0.89 | 9.5 |
| 22 | 45.493436 | −73.56647 | 2220.89 | 35 | 13 | 0.97 | 9 |
| 23 | 45.496555 | −73.57172 | 1236.33 | 30 | 100 | 0.96 | 9 |
| 24 | 45.477628 | −73.639895 | 6115.16 | 37 | 12 | 0.93 | 8.5 |
| 25 | 45.544292 | −73.764239 | 4334.49 | 40 | 8 | 0.94 | 9 |
| 26 | 45.430243 | −73.95103 | 1567.93 | 0 | 15 | 1 | 0 |
| 27 | 45.420916 | −73.946202 | 538.3 | 0 | 0 | 0 | 7.5 |
| 28 | 45.442709 | −73.603072 | 507.68 | 13 | 15 | 1 | 8 |
| 29 | 45.441032 | −73.609005 | 257.27 | 13 | 15 | 1 | 8 |
| 30 | 45.443038 | −73.596616 | 286.66 | 13 | 15 | 1 | 8 |
| 31 | 45.578561 | −73.711505 | 3574.49 | 40 | 11 | 0.95 | 7.5 |
| 32 | 45.620783 | −73.736125 | 1468.17 | 40 | 9 | 0.92 | 7.8 |
| 33 | 45.567735 | −73.773246 | 469 | 50 | 8 | 0.6 | 11 |
| 34 | 45.573021 | −73.775261 | 573.33 | 50 | 40 | 0.91 | 10 |
| 35 | 45.578094 | −73.726646 | 3343.3 | 75 | 8.5 | 0.8 | 9 |
| 36 | 45.606471 | −73.760197 | 981.7 | 0 | 15 | 1 | 0 |

**Table A1.** *Cont.*

| Zone | Latitude deg | Longitude deg | Radius m | $d_o$ m | $h_o$ m | $F$ | $h_L$ m |
|---|---|---|---|---|---|---|---|
| 37 | 45.608425 | −73.721034 | 1745.27 | 40 | 9.5 | 0.92 | 7.8 |
| 38 | 45.573973 | −73.732847 | 652.33 | 30 | 10 | 0.85 | 7.5 |
| 39 | 45.58667 | −73.71821 | 475.18 | 30 | 10.5 | 0.85 | 8 |
| 40 | 45.581243 | −73.712424 | 589.31 | 30 | 10.5 | 0.85 | 8 |
| 41 | 45.606794 | −73.678565 | 2757.33 | 40 | 11 | 0.95 | 7.5 |
| 42 | 45.499381 | −73.777284 | 1984.69 | 30 | 8 | 0.93 | 9 |
| 43 | 45.624484 | −73.777209 | 1028.74 | 30 | 8 | 0.93 | 9 |
| 44 | 45.626746 | −73.751446 | 1163.5 | 45 | 10 | 0.79 | 9 |
| 45 | 45.642074 | −73.759972 | 1111.32 | 45 | 10 | 0.79 | 9 |
| 46 | 45.654009 | −73.753926 | 565.21 | 45 | 10 | 0.79 | 9 |
| 47 | 45.628283 | −73.646522 | 864.23 | 100 | 9 | 0.79 | 9 |
| 48 | 45.636819 | −73.644179 | 704.06 | 100 | 9 | 0.79 | 9 |
| 49 | 45.669672 | −73.580719 | 1135.41 | 35 | 10.5 | 0.9 | 9 |
| 50 | 45.655778 | −73.594472 | 756.39 | 35 | 10.5 | 0.9 | 9 |
| 51 | 45.649959 | −73.610008 | 748.64 | 35 | 10.5 | 0.9 | 9 |
| 52 | 45.685863 | −73.593969 | 122.28 | 35 | 10 | 0.9 | 8 |
| 53 | 45.684019 | −73.59329 | 158.31 | 35 | 10 | 0.9 | 8 |
| 54 | 45.687316 | −73.624922 | 397.88 | 40 | 11 | 0.95 | 9 |
| 55 | 45.681938 | −73.626754 | 378.97 | 40 | 11 | 0.95 | 9 |
| 56 | 45.685351 | −73.640389 | 429.63 | 40 | 10.5 | 0.9 | 7.5 |
| 57 | 45.684927 | −73.644576 | 513.06 | 40 | 10.5 | 0.9 | 7.5 |
| 58 | 45.578662 | −73.810779 | 1885.89 | 40 | 9 | 0.92 | 7.5 |
| 59 | 45.669865 | −73.581445 | 1176.66 | 40 | 6 | 0.87 | 7 |
| 60 | 45.658336 | −73.595139 | 486.99 | 40 | 6 | 0.87 | 7 |
| 61 | 45.649695 | −73.607701 | 943.64 | 40 | 6 | 0.87 | 7 |
| 62 | 45.619713 | −73.736748 | 1577.7 | 40 | 9.5 | 0.92 | 7.8 |
| 63 | 45.605547 | −73.802901 | 395.48 | 30 | 8 | 0.93 | 9 |
| 64 | 45.605643 | −73.806192 | 170.05 | 93 | 6.5 | 0.86 | 20 |
| 65 | 45.603383 | −73.805732 | 177.03 | 93 | 6.5 | 0.86 | 20 |
| 66 | 45.601263 | −73.806303 | 138.59 | 93 | 6.5 | 0.86 | 20 |
| 67 | 45.596595 | −73.80829 | 285.24 | 75 | 7 | 0.35 | 5 |
| 68 | 45.589523 | −73.817458 | 598.77 | 40 | 8 | 0.98 | 7.5 |
| 69 | 45.579687 | −73.785752 | 519.3 | 80 | 9 | 0.91 | 10 |
| 70 | 45.566742 | −73.794239 | 956.48 | 95 | 9.5 | 0.86 | 9 |
| 71 | 45.564699 | −73.783424 | 534.76 | 95 | 9.5 | 0.86 | 9 |
| 72 | 45.57769 | −73.809499 | 1685.56 | 40 | 8 | 0.98 | 7.5 |
| 73 | 45.57275 | −73.779812 | 407.35 | 40 | 9 | 0.92 | 6.5 |
| 74 | 45.576025 | −73.769727 | 434.77 | 40 | 9 | 0.92 | 6.5 |
| 75 | 45.577226 | −73.76237 | 277.36 | 40 | 9 | 0.92 | 6.5 |
| 76 | 45.572138 | −73.772153 | 177.08 | 40 | 9 | 0.92 | 6.5 |
| 77 | 45.534093 | −73.788879 | 370.15 | 95 | 7.5 | 0.78 | 8 |
| 78 | 45.530072 | −73.784738 | 373.43 | 95 | 7.5 | 0.78 | 8 |
| 79 | 45.526837 | −73.780306 | 386.65 | 95 | 7.5 | 0.78 | 8 |
| 80 | 45.493572 | −73.824689 | 2915.16 | 43 | 11 | 0.93 | 8 |
| 81 | 45.44632 | −73.841687 | 5030.89 | 43 | 11 | 0.93 | 8 |
| 82 | 45.413312 | −73.900346 | 1294.62 | 43 | 11 | 0.93 | 8 |
| 83 | 45.405117 | −73.920945 | 1287.47 | 43 | 11 | 0.93 | 8 |
| 84 | 45.436933 | −73.92663 | 485.53 | 43 | 11 | 0.93 | 8 |
| 85 | 45.414199 | −73.958716 | 739.01 | 43 | 11 | 0.93 | 8 |
| 86 | 45.447606 | −73.773278 | 1300.58 | 43 | 11 | 0.93 | 8 |

**Table A1.** *Cont.*

| Zone | Latitude deg | Longitude deg | Radius m | $d_o$ m | $h_o$ m | $F$ | $h_L$ m |
|---|---|---|---|---|---|---|---|
| 87 | 45.437128 | −73.74873 | 1303.57 | 43 | 11 | 0.93 | 8 |
| 88 | 45.437151 | −73.728026 | 1303.57 | 43 | 11 | 0.93 | 8 |
| 89 | 45.436428 | −73.712233 | 1303.57 | 43 | 11 | 0.93 | 8 |
| 90 | 45.435847 | −73.694037 | 1303.57 | 43 | 11 | 0.93 | 8 |
| 91 | 45.461948 | −73.706166 | 1638.72 | 65 | 7 | 0.87 | 9.5 |
| 92 | 45.451977 | −73.735921 | 1365.22 | 65 | 7 | 0.87 | 9.5 |
| 93 | 45.489822 | −73.67055 | 938.96 | 65 | 6 | 0.85 | 9 |
| 94 | 45.489412 | −73.685756 | 580.2 | 65 | 6 | 0.85 | 9 |
| 95 | 45.483317 | −73.699904 | 1126.54 | 65 | 6 | 0.85 | 9 |
| 96 | 45.494602 | −73.713477 | 1121.04 | 65 | 6 | 0.85 | 9 |
| 97 | 45.493228 | −73.727198 | 1016.49 | 65 | 6 | 0.85 | 9 |
| 98 | 45.496296 | −73.747347 | 1345.71 | 65 | 6 | 0.85 | 9 |
| 99 | 45.483364 | −73.771305 | 1218.45 | 65 | 6 | 0.85 | 9 |
| 100 | 45.480148 | −73.787168 | 719.05 | 65 | 6 | 0.85 | 9 |
| 101 | 45.477018 | −73.797811 | 860.89 | 65 | 6 | 0.85 | 9 |
| 102 | 45.472685 | −73.810858 | 737.6 | 65 | 6 | 0.85 | 9 |
| 103 | 45.467943 | −73.820363 | 740.19 | 65 | 6 | 0.85 | 9 |
| 104 | 45.46204 | −73.829461 | 633.07 | 65 | 6 | 0.85 | 9 |
| 105 | 45.455371 | −73.841071 | 587.43 | 65 | 6 | 0.85 | 9 |
| 106 | 45.452773 | −73.853174 | 434.61 | 65 | 6 | 0.85 | 9 |
| 107 | 45.450889 | −73.859754 | 177.03 | 65 | 6 | 0.85 | 9 |
| 108 | 45.449305 | −73.862786 | 177.03 | 65 | 6 | 0.85 | 9 |
| 109 | 45.447943 | −73.866002 | 177.03 | 65 | 6 | 0.85 | 9 |
| 110 | 45.446649 | −73.870508 | 274.22 | 65 | 6 | 0.85 | 9 |
| 111 | 45.444361 | −73.875338 | 273.59 | 65 | 6 | 0.85 | 9 |
| 112 | 45.44284 | −73.880347 | 230.01 | 65 | 6 | 0.85 | 9 |
| 113 | 45.440791 | −73.889868 | 293.27 | 65 | 6 | 0.85 | 9 |
| 114 | 45.458772 | −73.905955 | 488.75 | 43 | 11 | 0.93 | 8 |
| 115 | 45.402525 | −73.946758 | 1367.94 | 43 | 11 | 0.93 | 8 |
| 116 | 45.427927 | −73.905635 | 516.35 | 85 | 11 | 0.82 | 9 |
| 117 | 45.425306 | −73.911214 | 441.22 | 85 | 11 | 0.82 | 9 |
| 118 | 45.421662 | −73.918981 | 407.7 | 85 | 11 | 0.82 | 9 |
| 119 | 45.418576 | −73.927174 | 442.58 | 85 | 11 | 0.82 | 9 |
| 120 | 45.422483 | −73.928008 | 337.96 | 85 | 11 | 0.82 | 9 |
| 121 | 45.430551 | −73.922325 | 339.98 | 85 | 11 | 0.82 | 9 |
| 122 | 45.439212 | −73.67468 | 910.53 | 37 | 8 | 0.92 | 8 |
| 123 | 45.506652 | −73.595021 | 946.73 | 15 | 15 | 1 | 8 |
| 124 | 45.501238 | −73.603776 | 976.3 | 15 | 15 | 1 | 8 |
| 125 | 45.479753 | −73.555974 | 489.03 | 35 | 13 | 0.97 | 9 |
| 126 | 45.477135 | −73.573088 | 1174.82 | 35 | 13 | 0.97 | 9 |
| 127 | 45.469233 | −73.577894 | 1576.84 | 35 | 13 | 0.97 | 9 |
| 128 | 45.455685 | −73.578583 | 1402.7 | 35 | 13 | 0.97 | 9 |
| 129 | 45.455324 | −73.594204 | 1174.42 | 35 | 13 | 0.97 | 9 |
| 130 | 45.441617 | −73.605908 | 1939.18 | 35 | 10 | 0.94 | 9 |
| 131 | 45.430776 | −73.623245 | 2212.91 | 35 | 10 | 0.94 | 9 |
| 132 | 45.430535 | −73.659809 | 1389.83 | 35 | 10 | 0.94 | 9 |
| 133 | 45.443726 | −73.595941 | 241.4 | 2 | 15 | 1 | 0 |
| 134 | 45.442281 | −73.603322 | 544.94 | 2 | 15 | 1 | 0 |
| 135 | 45.441619 | −73.611304 | 119.46 | 2 | 15 | 1 | 0 |
| 136 | 45.440414 | −73.613536 | 112.65 | 2 | 15 | 1 | 0 |

**Table A1.** *Cont.*

| Zone | Latitude deg | Longitude deg | Radius m | $d_o$ m | $h_o$ m | $F$ | $h_L$ m |
|---|---|---|---|---|---|---|---|
| 137 | 45.439993 | −73.610961 | 112.65 | 2 | 15 | 1 | 0 |
| 138 | 45.511098 | −73.687745 | 1808.9 | 40 | 11 | 0.93 | 8 |
| 139 | 45.516511 | −73.724591 | 1734.61 | 40 | 11 | 0.93 | 8 |
| 140 | 45.531184 | −73.6977 | 1821.15 | 40 | 11 | 0.93 | 8 |
| 141 | 45.537967 | −73.680233 | 1243.1 | 40 | 11 | 0.93 | 8 |
| 142 | 45.540624 | −73.652515 | 763.8 | 65 | 9 | 0.93 | 9 |
| 143 | 45.532847 | −73.657335 | 756.39 | 65 | 9 | 0.93 | 9 |
| 144 | 45.534852 | −73.628654 | 371.56 | 100 | 15 | 0.3 | 17 |
| 145 | 45.532056 | −73.587713 | 178.69 | 10 | 15 | 1 | 17 |
| 146 | 45.526945 | −73.568316 | 297.51 | 10 | 15 | 1 | 17 |
| 147 | 45.524484 | −73.567667 | 193.12 | 10 | 15 | 1 | 17 |
| 148 | 45.525882 | −73.570865 | 192.76 | 10 | 15 | 1 | 17 |
| 149 | 45.538685 | −73.590452 | 142.93 | 100 | 15 | 0.3 | 40 |
| 150 | 45.539332 | −73.5941 | 188.34 | 100 | 15 | 0.3 | 5 |
| 151 | 45.562269 | −73.625156 | 519.59 | 0 | 0 | 0 | 7.5 |
| 152 | 45.564913 | −73.633868 | 483.82 | 0 | 0 | 0 | 7.5 |
| 153 | 45.569832 | −73.613291 | 144.84 | 0 | 0 | 0 | 0 |
| 154 | 45.572223 | −73.615995 | 289.68 | 0 | 0 | 0 | 0 |
| 155 | 45.574607 | −73.61108 | 296.16 | 0 | 0 | 0 | 0 |
| 156 | 45.576691 | −73.623896 | 209.21 | 0 | 0 | 0 | 0 |
| 157 | 45.577986 | −73.626797 | 209.21 | 0 | 0 | 0 | 0 |
| 158 | 45.579337 | −73.630016 | 203.59 | 0 | 0 | 0 | 0 |
| 159 | 45.563097 | −73.562043 | 603.88 | 50 | 15 | 0.5 | 0 |
| 160 | 45.569076 | −73.556293 | 354.04 | 50 | 15 | 0.5 | 0 |
| 161 | 45.56661 | −73.545697 | 628.63 | 150 | 9 | 0.85 | 10 |
| 162 | 45.564507 | −73.531449 | 627.64 | 30 | 9 | 0.85 | 10 |
| 163 | 45.578913 | −73.51808 | 1034.25 | 30 | 9 | 0.85 | 10 |
| 164 | 45.587119 | −73.544519 | 266.44 | 100 | 15 | 0.2 | 0 |
| 165 | 45.588011 | −73.548111 | 241.4 | 100 | 15 | 0.2 | 0 |
| 166 | 45.5889213 | −73.552403 | 241.4 | 100 | 15 | 0.2 | 0 |
| 167 | 45.590504 | −73.55618 | 237.65 | 100 | 15 | 0.2 | 0 |
| 168 | 45.589963 | −73.561347 | 112.65 | 100 | 15 | 0.2 | 0 |
| 169 | 45.590414 | −73.563085 | 109.74 | 100 | 15 | 0.2 | 0 |
| 170 | 45.591149 | −73.565703 | 141.11 | 100 | 15 | 0.2 | 0 |
| 171 | 45.593125 | −73.568101 | 153.25 | 100 | 15 | 0.2 | 0 |
| 172 | 45.617099 | −73.604364 | 370.15 | 75 | 15 | 0.7 | 20 |
| 173 | 45.619891 | −73.607488 | 374.1 | 75 | 15 | 0.7 | 20 |
| 174 | 45.622322 | −73.61063 | 358.69 | 75 | 15 | 0.7 | 12 |
| 175 | 45.425901 | −73.612466 | 261.16 | 75 | 15 | 0.7 | 12 |
| 176 | 45.601307 | −73.610067 | 370.15 | 65 | 8 | 0.95 | 9 |
| 177 | 45.606351 | −73.604574 | 443.68 | 65 | 8 | 0.95 | 9 |
| 178 | 45.601908 | −73.589897 | 403.82 | 65 | 8 | 0.95 | 9 |
| 179 | 45.599265 | −73.583202 | 402.33 | 65 | 8 | 0.95 | 9 |
| 180 | 45.595563 | −73.574813 | 402.33 | 65 | 8 | 0.95 | 9 |
| 181 | 45.599987 | −73.564625 | 402.33 | 65 | 8 | 0.95 | 9 |
| 182 | 45.617505 | −73.573595 | 1384.72 | 65 | 8 | 0.95 | 9 |
| 183 | 45.642984 | −73.564979 | 520.76 | 65 | 8 | 0.95 | 9 |
| 184 | 45.647244 | −73.557512 | 514.99 | 65 | 8 | 0.95 | 9 |
| 185 | 45.650664 | −73.550713 | 514.99 | 65 | 8 | 0.95 | 9 |
| 186 | 45.653797 | −73.544229 | 514.99 | 65 | 8 | 0.95 | 9 |

**Table A1.** *Cont.*

| Zone | Latitude deg | Longitude deg | Radius m | $d_o$ m | $h_o$ m | $F$ | $h_L$ m |
|---|---|---|---|---|---|---|---|
| 187 | 45.652699 | −73.520683 | 847.72 | 65 | 8 | 0.95 | 9 |
| 188 | 45.645286 | −73.515518 | 245.1 | 65 | 8 | 0.95 | 9 |
| 189 | 45.629559 | −73.565273 | 553.62 | 0 | 15 | 1 | 0 |
| 190 | 45.627203 | −73.560413 | 473.68 | 0 | 0 | 0 | 15 |
| 191 | 45.634786 | −73.540334 | 2026.09 | 110 | 15 | 0.5 | 9 |
| 192 | 45.635317 | −73.511496 | 397.62 | 110 | 15 | 0.5 | 9 |
| 193 | 45.653453 | −73.580984 | 112.65 | 0 | 15 | 1 | 0 |
| 194 | 45.650783 | −73.574353 | 112.65 | 0 | 15 | 1 | 0 |
| 195 | 45.649181 | −73.572868 | 115.85 | 0 | 15 | 1 | 0 |
| 196 | 45.665821 | −73.52684 | 767.75 | 0 | 0 | 0 | 7.5 |
| 197 | 45.669147 | −73.493507 | 979.45 | 40 | 11 | 0.93 | 8 |
| 198 | 45.682365 | −73.496987 | 981.7 | 40 | 11 | 0.93 | 8 |
| 199 | 45.695915 | −73.48791 | 981.7 | 40 | 11 | 0.93 | 8 |
| 200 | 45.680895 | −73.497232 | 340.81 | 0 | 15 | 1 | 0 |
| 201 | 45.670026 | −73.514763 | 291.6 | 0 | 15 | 1 | 0 |
| 202 | 45.676246 | −73.512102 | 418.06 | 0 | 15 | 1 | 0 |
| 203 | 45.680905 | −73.512188 | 292.68 | 0 | 15 | 1 | 0 |
| 204 | 45.431493 | −73.894652 | 572.65 | 0 | 15 | 1 | 0 |
| 205 | 45.439319 | −73.913471 | 728.19 | 0 | 15 | 1 | 0 |
| 206 | 45.443898 | −73.924428 | 415.84 | 0 | 15 | 1 | 0 |
| 207 | 45.450941 | −73.928406 | 545.9 | 0 | 15 | 1 | 0 |
| 208 | 45.46597 | −73.9361 | 1308.31 | 0 | 15 | 1 | 0 |
| 209 | 45.40949 | −73.483236 | 2031.04 | 40 | 11 | 0.93 | 7.5 |
| 210 | 45.460311 | −73.919206 | 462.48 | 43 | 11 | 0.9 | 8 |
| 211 | 45.384537 | −73.567484 | 2654.36 | 40 | 11 | 0.93 | 7.5 |
| 212 | 45.38829 | −73.517825 | 2391.21 | 40 | 11 | 0.93 | 7.5 |
| 213 | 45.365836 | −73.510154 | 497.23 | 40 | 11 | 0.93 | 7.5 |
| 214 | 45.368097 | −73.488407 | 612.36 | 40 | 11 | 0.93 | 7.5 |
| 215 | 45.375095 | −73.490862 | 359.86 | 40 | 11 | 0.93 | 7.5 |
| 216 | 45.383713 | −73.466433 | 528.53 | 40 | 11 | 0.93 | 7.5 |
| 217 | 45.390115 | −73.486617 | 198.1 | 40 | 11 | 0.93 | 7.5 |
| 218 | 45.392521 | −73.482472 | 269.4 | 40 | 11 | 0.93 | 7.5 |
| 219 | 45.401296 | −73.594288 | 1028.76 | 45 | 7 | 0.7 | 13 |
| 220 | 45.39903 | −73.512902 | 1029.98 | 60 | 7 | 0.85 | 13 |
| 221 | 45.398829 | −73.498305 | 620.73 | 60 | 7 | 0.85 | 13 |
| 222 | 45.405579 | −73.487061 | 627.64 | 0 | 0 | 0 | 7.5 |
| 223 | 45.44346 | −73.466336 | 2336.13 | 40 | 11 | 0.93 | 7.5 |
| 224 | 45.491615 | −73.455755 | 5334.41 | 40 | 11 | 0.93 | 7.5 |
| 225 | 45.504905 | −73.380228 | 741.55 | 40 | 11 | 0.93 | 7.5 |
| 226 | 45.526102 | −73.345277 | 2616.82 | 40 | 11 | 0.93 | 7.5 |
| 227 | 45.525959 | −73.501946 | 2114.48 | 40 | 11 | 0.93 | 7.5 |
| 228 | 45.557552 | −73.458245 | 3794.15 | 40 | 11 | 0.93 | 7.5 |
| 229 | 45.592847 | −73.430247 | 3707.6 | 40 | 11 | 0.93 | 7.5 |
| 230 | 45.589204 | −73.345012 | 2024.99 | 40 | 11 | 0.93 | 7.5 |
| 231 | 45.62611 | −73.448933 | 1376.51 | 40 | 11 | 0.93 | 7.5 |
| 232 | 45.661787 | −73.430983 | 1059.7 | 40 | 11 | 0.93 | 7.5 |
| 233 | 45.682631 | −73.42627 | 1757.84 | 40 | 11 | 0.93 | 7.5 |
| 234 | 45.572432 | −73.464773 | 1573.29 | 60 | 9 | 0.96 | 9 |
| 235 | 45.567145 | −73.442114 | 640.6 | 60 | 9 | 0.96 | 9 |
| 236 | 45.562097 | −73.425977 | 1071.75 | 60 | 9 | 0.96 | 9 |

**Table A1.** *Cont.*

| Zone | Latitude deg | Longitude deg | Radius m | $d_o$ m | $h_o$ m | $F$ | $h_L$ m |
|---|---|---|---|---|---|---|---|
| 237 | 45.548221 | −73.466156 | 532.35 | 0 | 15 | 1 | 0 |
| 238 | 45.55182 | −73.471725 | 501.56 | 0 | 15 | 1 | 0 |
| 239 | 45.544908 | −73.429411 | 1112.15 | 0 | 15 | 1 | 0 |
| 240 | 45.601691 | −73.396831 | 1332.24 | 0 | 15 | 1 | 0 |
| 241 | 45.620184 | −73.411938 | 1952.5 | 0 | 0 | 0 | 7.5 |
| 242 | 45.590527 | −73.430877 | 241.4 | 65 | 11 | 0.9 | 8 |
| 243 | 45.593777 | −73.434972 | 248.7 | 65 | 11 | 0.9 | 8 |
| 244 | 45.53419 | −73.851753 | 537.21 | 80 | 15 | 1 | 0 |
| 245 | 45.531666 | −73.848724 | 531.08 | 80 | 15 | 1 | 0 |
| 246 | 45.525668 | −73.847035 | 236.5 | 80 | 15 | 1 | 0 |
| 247 | 45.530092 | −73.87059 | 609.58 | 80 | 15 | 1 | 0 |
| 248 | 45.583708 | −73.853991 | 819.97 | 35 | 11 | 0.93 | 8.5 |
| 249 | 45.639335 | −73.844072 | 2524.36 | 35 | 10 | 0.93 | 9 |
| 250 | 45.612433 | −73.840306 | 1346.83 | 35 | 11 | 0.93 | 7 |
| 251 | 45.620875 | −73.867936 | 1181.61 | 35 | 10 | 0.93 | 4 |
| 252 | 45.63086 | −73.819304 | 395.32 | 150 | 8 | 0.7 | 12 |
| 253 | 45.626125 | −73.833429 | 294.62 | 65 | 8 | 0.91 | 10 |
| 254 | 45.622643 | −73.828451 | 289.68 | 65 | 8 | 0.91 | 10 |
| 255 | 45.638235 | −73.871145 | 823.41 | 90 | 8.5 | 0.92 | 9.5 |
| 256 | 45.635457 | −73.860373 | 613.65 | 90 | 8.5 | 0.92 | 9.5 |
| 257 | 45.628755 | −73.848429 | 611.55 | 185 | 8.5 | 0.7 | 13 |
| 258 | 45.644005 | −73.839829 | 402.33 | 75 | 15 | 0.85 | 10 |
| 259 | 45.62046 | −73.811862 | 1017.72 | 35 | 11 | 0.93 | 7.5 |
| 260 | 45.650328 | −73.786076 | 1171.49 | 35 | 11 | 0.93 | 4.5 |
| 261 | 45.640103 | −73.796167 | 1351.87 | 35 | 11 | 0.93 | 7.5 |
| 262 | 45.685073 | −73.770836 | 3167.5 | 35 | 10 | 0.93 | 8 |
| 263 | 45.686239 | −73.764711 | 781.05 | 80 | 8 | 0.91 | 9 |
| 264 | 45.693831 | −73.754997 | 454.89 | 80 | 8 | 0.91 | 9 |
| 265 | 45.685292 | −73.781511 | 450.62 | 65 | 8 | 0.91 | 9 |
| 266 | 45.732301 | −73.651759 | 4943.41 | 35 | 10 | 0.93 | 8 |
| 267 | 45.717773 | −73.617568 | 435.69 | 60 | 8 | 0.91 | 8 |
| 268 | 45.711828 | −73.622 | 341.12 | 60 | 8 | 0.91 | 8 |
| 269 | 45.723656 | −73.616404 | 485.45 | 130 | 8 | 0.75 | 13 |
| 270 | 45.728241 | −73.67683 | 310.54 | 65 | 9 | 0.91 | 8.5 |
| 271 | 45.726383 | −73.68301 | 252.41 | 65 | 9 | 0.91 | 8.5 |
| 272 | 45.724885 | −73.689161 | 270.88 | 65 | 9 | 0.91 | 8.5 |
| 273 | 45.72099 | −73.701264 | 500.39 | 100 | 9 | 0.88 | 8.5 |
| 274 | 45.718185 | −73.709356 | 321.87 | 100 | 9 | 0.88 | 8.5 |
| 275 | 45.723627 | −73.69517 | 318.72 | 65 | 9 | 0.91 | 8.5 |
| 276 | 45.715044 | −73.715202 | 386.24 | 100 | 9 | 0.88 | 8.5 |
| 277 | 45.711868 | −73.721554 | 386.24 | 100 | 9 | 0.88 | 8.5 |
| 278 | 45.706062 | −73.719135 | 386.24 | 100 | 9 | 0.88 | 8.5 |
| 279 | 45.702607 | −73.725064 | 391.93 | 100 | 9 | 0.88 | 8.5 |
| 280 | 45.694093 | −73.601574 | 708.11 | 35 | 10 | 0.93 | 8 |
| 281 | 45.701072 | −73.58597 | 1021.75 | 35 | 10 | 0.93 | 8 |
| 282 | 45.704059 | −73.552405 | 460.06 | 35 | 10 | 0.93 | 8 |
| 283 | 45.780634 | −73.629427 | 715.04 | 40 | 7.5 | 0.94 | 7 |
| 284 | 45.717937 | −73.512757 | 1813.91 | 250 | 7.5 | 0.7 | 15 |
| 285 | 45.715355 | −73.499264 | 393.32 | 35 | 10 | 0.93 | 4.5 |
| 286 | 45.709849 | −73.518397 | 708.11 | 35 | 9 | 0.93 | 7 |

**Table A1.** *Cont.*

| Zone | Latitude deg | Longitude deg | Radius m | $d_o$ m | $h_o$ m | $F$ | $h_L$ m |
|---|---|---|---|---|---|---|---|
| 287 | 45.721475 | −73.517882 | 700.18 | 35 | 9 | 0.93 | 4.5 |
| 288 | 45.725952 | −73.507309 | 491.42 | 150 | 25 | 0.7 | 12 |
| 289 | 45.358039 | −73.736125 | 3138.21 | 35 | 8 | 0.93 | 7 |
| 290 | 45.347865 | −73.686877 | 1096.88 | 70 | 9 | 0.91 | 9 |
| 291 | 45.366609 | −73.710982 | 305.75 | 80 | 8 | 0.75 | 8.5 |
| 292 | 45.363505 | −73.712964 | 110.71 | 80 | 8 | 0.75 | 8.5 |
| 293 | 45.361562 | −73.713524 | 129.44 | 80 | 8 | 0.75 | 8.5 |
| 294 | 45.359212 | −73.715659 | 158.96 | 80 | 8 | 0.75 | 8.5 |
| 295 | 45.358528 | −73.719093 | 110.58 | 150 | 10 | 0.7 | 10 |
| 296 | 45.358851 | −73.722002 | 122.72 | 150 | 10 | 0.7 | 10 |
| 297 | 45.359026 | −73.72511 | 128.75 | 150 | 10 | 0.7 | 10 |
| 298 | 45.359377 | −73.728149 | 111.96 | 150 | 10 | 0.7 | 10 |
| 299 | 45.359779 | −73.731011 | 112.65 | 150 | 10 | 0.7 | 10 |
| 300 | 45.360172 | −73.733924 | 112.65 | 150 | 10 | 0.7 | 10 |
| 301 | 45.356791 | −73.7169 | 144.32 | 80 | 8 | 0.75 | 8.5 |
| 302 | 45.35474 | −73.718359 | 111.27 | 80 | 8 | 0.75 | 8.5 |
| 303 | 45.35275 | −73.719475 | 112.65 | 80 | 8 | 0.75 | 8.5 |
| 304 | 45.351001 | −73.720419 | 112.65 | 80 | 8 | 0.75 | 8.5 |
| 305 | 45.342896 | −73.765213 | 634.29 | 150 | 25 | 0.7 | 12 |
| 306 | 45.356592 | −73.758567 | 144.84 | 40 | 12 | 0.93 | 5.5 |
| 307 | 45.357255 | −73.755048 | 139.51 | 80 | 7 | 0.7 | 11.5 |
| 308 | 45.410403 | −73.671463 | 956.46 | 35 | 7 | 0.93 | 7 |
| 309 | 45.411084 | −73.689762 | 949.51 | 35 | 7 | 0.93 | 7 |

## References


1. Van Geffen, K.G.; Groot, A.T.; Van Grunsven, R.H.; Donners, M.; Berendse, F.; Veenendaal, E.M. Artificial night lighting disrupts sex pheromone in a noctuid moth. *Ecol. Entomol.* **2015**, *40*, 401–408. [CrossRef]
2. Boldogh, S.; Dobrosi, D.; Samu, P. The effects of the illumination of buildings on house-dwelling bats and its conservation consequences. *Acta Chiropterologica* **2007**, *9*, 527–534. [CrossRef]
3. Kamrowski, R.L.; Limpus, C.; Pendoley, K.; Hamann, M. Influence of industrial light pollution on the sea-finding behaviour of flatback turtle hatchlings. *Wildl. Res.* **2015**, *41*, 421–434. [CrossRef]
4. Brüning, A.; Hölker, F.; Wolter, C. Artificial light at night: Implications for early life stages development in four temperate freshwater fish species. *Aquat. Sci.* **2011**, *73*, 143–152. [CrossRef]
5. Da Silva, A.; Valcu, M.; Kempenaers, B. Light pollution alters the phenology of dawn and dusk singing in common European songbirds. *Philos. Trans. R. Soc. Lond. B Biol. Sci.* **2015**, *370*, 1–2. [CrossRef]
6. Briggs, W.R. Physiology of plant responses to artificial lighting. In *Ecological Consequences of Artificial Night Lighting*; Island Press: Washington DC, USA, 2016; pp. 281–304.
7. Ffrench-Constant, R.H.; Somers-Yeates, R.; Bennie, J.; Economou, T.; Hodgson, D.; Spalding, A.; McGregor, P.K. Light pollution is associated with earlier tree budburst across the United Kingdom. *Proc. R. Soc. B Biol. Sci.* **2016**, *283*, 20160813. [CrossRef] [PubMed]
8. Bennie, J.; Davies, T.W.; Cruse, D.; Gaston, K.J. Ecological effects of artificial light at night on wild plants. *J. Ecol.* **2016**, *104*, 611–620. [CrossRef]
9. Škvareninová, J.; Tuhárska, M.; Škvarenina, J.; Babálová, D.; Slobodníková, L.; Slobodník, B.; Středová, H.; Mind'aš, J. Effects of light pollution on tree phenology in the urban environment. *Morav. Geogr. Rep.* **2017**, *25*, 282–290. [CrossRef]
10. Bennie, J.; Davies, T.W.; Cruse, D.; Bell, F.; Gaston, K.J. Artificial light at night alters grassland vegetation species composition and phenology. *J. Appl. Ecol.* **2018**, *55*, 442–450. [CrossRef]
11. Kloog, I.; Haim, A.; Stevens, R.G.; Portnov, B.A. Global Co-Distribution of Light at Night (LAN) and Cancers of Prostate, Colon, and Lung in Men. *Chronobiol. Int.* **2009**, *26*, 108–125. [CrossRef]
12. Kloog, I.; Haim, A.; Stevens, R.G.; Barchana, M.; Portnov, B.A. Light at Night Co-distributes with Incident Breast but not Lung Cancer in the Female Population of Israel. *Chronobiol. Int.* **2008**, *25*, 65–81. [CrossRef] [PubMed]
13. Stevens, R.G. Light-at-night, circadian disruption and breast cancer: Assessment of existing evidence. *Int. J. Epidemiol.* **2009**, *38*, 963–970. [CrossRef] [PubMed]

14. Benke, K.E.; Benke, K.K.; Dimitriadis, C. Spectral content of artificial lighting and effects on health. *J. Australas. Coll. Nutr. Environ. Med.* **2011**, *30*, 13.
15. Cajochen, C.; Altanay-Ekici, S.; Münch, M.; Frey, S.; Knoblauch, V.; Wirz-Justice, A. Evidence that the lunar cycle influences human sleep. *Curr. Biol.* **2013**, *23*, 1485–1488. [CrossRef] [PubMed]
16. Garaulet, M.; Ordovas, J.M. *Chronobiology and Obesity*; Springer: New York, NY, USA, 2013; pp. 133–160.
17. Aubé, M.; Roby, J.; Kocifaj, M. Evaluating Potential Spectral Impacts of Various Artificial Lights on Melatonin Suppression, Photosynthesis, and Star Visibility. *PLoS ONE* **2013**, *20*, e67798. [CrossRef]
18. Garcia-Saenz, A.; Sánchez de Miguel, A.; Espinosa, A.; Valentin, A.; Aragonés, N.; Llorca, J.; Amiano, P.; Martín Sánchez, V.; Guevara, M.; Capelo, R.; et al. Evaluating the association between artificial light-at-night exposure and breast and prostate cancer risk in Spain (MCC-Spain study). *Environ. Health Perspect.* **2018**, *126*, 047011. [CrossRef] [PubMed]
19. Garcia-Saenz, A.; de Miguel, A.S.; Espinosa, A.; Costas, L.; Aragonés, N.; Tonne, C.; Moreno, V.; Pérez-Gómez, B.; Valentin, A.; Pollán, M.; et al. Association between outdoor light-at-night exposure and colorectal cancer in Spain. *Epidemiology* **2020**, *31*, 718–727. [CrossRef] [PubMed]
20. Garstang, R.H. Model for artificial night-sky illumination. *Publ. Astron. Soc. Pac.* **1986**, *98*, 364–375. [CrossRef]
21. Luginbuhl, C.B.; Duriscoe, D.M.; Moore, C.W.; Richman, A.; Lockwood, W.G.; Davis, D.R. From the ground up II: Sky glow and near-ground artificial light propagation in Flagstaff, Arizona. *Publ. Astron. Soc. Pac.* **2009**, *121*, 204–212. [CrossRef]
22. Cinzano, P.; Falchi, F. The propagation of light pollution in the atmosphere. *Mon. Not. R. Astron. Soc.* **2012**, *427*, 3337–3357. [CrossRef]
23. Aubé, M.; Franchomme-Fossé, L.; Robert-Staehler, P.; Houle, V. Light pollution modelling and detection in a heterogeneous environment: Toward a night-time aerosol optical depth retrieval method. In *Optics & Photonics 2005*; International Society for Optics and Photonics: Bellingham, WA, USA, 2005; p. 589012.
24. Kocifaj, M. Light-pollution model for cloudy and cloudless night skies with ground-based light sources. *Appl. Opt.* **2007**, *46*, 3013–3022. [CrossRef] [PubMed]
25. Aubé, M. Light pollution models and detection method take account of heterogeneous environments. *SPIE Newsroom* **2006**. [CrossRef]
26. Aubé, M.; Simoneau, A. New features to the night sky radiance model illumina: Hyperspectral support, improved obstacles and cloud reflection. *J. Quant. Spectrosc. Radiat. Transf.* **2018**, *211*, 25–34. [CrossRef]
27. Aubé, M.; Simoneau, A.; Muñoz-Tuñón, C.; Díaz-Castro, J.; Serra-Ricart, M. Restoring the night sky darkness at Observatorio del Teide: First application of the model Illumina version 2. *Mon. Not. R. Astron. Soc.* **2020**, *497*, 2501–2516. [CrossRef]
28. Aubé, M.; Simoneau, A. Illumina Webpage. 2021. Available online: https://lx02.cegepsherbrooke.qc.ca/~aubema/index.php/Prof/IllumEn (accessed on 30 May 2021).
29. Aubé, M.; Roby, J. Sky brightness levels before and after the creation of the first International Dark Sky Reserve, Mont-Mégantic Observatory, Québec, Canada. *J. Quant. Spectrosc. Radiat. Transf.* **2014**, *139*, 52–63. [CrossRef]
30. Aubé, M. Physical behaviour of anthropogenic light propagation into the nocturnal environment. *Phil. Trans. R. Soc. B* **2015**, *370*, 20140117. [CrossRef]
31. Statistics Canada. Census 2016. Available online: https://www12.statcan.gc.ca/census-recensement/2016/dp-pd/prof/details/page.cfm?lang=E&Geo1=CSD&Code1=2466023&Geo2=PR&Code2=24&SearchText=Montreal&SearchType=Begins&SearchPR=01&B1=All&GeoLevel=PR&GeoCode=2466023&TABID=1&type=0 (accessed on 30 May 2021)
32. SkyscraperPage.com. Montreal Skyscraper Diagram. 2017. Available online: https://skyscraperpage.com/diagrams/?cityID=22 (accessed on 30 May 2021).
33. Simoneau, A.; Aubé, M.; Bertolo, A. Multispectral analysis of the night sky brightness and its origin for the Asiago Observatory, Italy. *Mon. Not. R. Astron. Soc.* **2020**, *491*, 4398–4405. [CrossRef]
34. Government of Canada. Canadian Climate Normals 1971–2000 Station Data. 2015. Available online: climate.weather.gc.ca/climate_normals/results_e.html?stnID=5415&lang=f&StationName=montreal&SearchType=Contains&stnNameSubmit=go&dCode=1 (accessed on 30 May 2021).
35. AERONET. AERONET Data Display Interface. 2021. Available online: aeronet.gsfc.nasa.gov (accessed on 30 May 2021).
36. Shettle, E.P.; Fenn, R.W. Models for the Aerosols of the Lower Atmosphere and the Effects of Humidity Variations on Their Optical Properties. *Environ. Res. Pap.* **1979**, *676*, 89.
37. Farr, T.G.; Rosen, P.A.; Caro, E.; Crippen, R.; Duren, R.; Hensley, S.; Kobrick, M.; Paller, M.; Rodriguez, E.; Roth, L.; et al. The shuttle radar topography mission. *Rev. Geophys.* **2007**, *45*. [CrossRef]
38. de Miguel, A.S.; Kyba, C.C.; Aubé, M.; Zamorano, J.; Cardiel, N.; Tapia, C.; Bennie, J.; Gaston, K.J. Colour remote sensing of the impact of artificial light at night (I): The potential of the International Space Station and other DSLR-based platforms. *Remote Sens. Environ.* **2019**, *224*, 92–103. [CrossRef]
39. de Miguel, S. NOKTOsat Website. 2021. Available online: http://noktosat.com (accessed on 30 May 2021).
40. Elvidge, C.D.; Baugh, K.; Zhizhin, M.; Hsu, F.C.; Ghosh, T. VIIRS night-time lights. *Int. J. Remote Sens.* **2017**, *38*, 5860–5879. [CrossRef]
41. Roby, J.; Aubé, M.; Morin Paulhus, A. LSPDD: Lamp Spectral Power Distribution Database. 2021. Available online: https://lspdd.org (accessed on 30 May 2021).
42. Google Maps. Google Maps. 2021. Available online: https://www.google.ca/maps (accessed on 30 May 2021).

43. Google Earth. Google Earth. 2021. Available online: https://www.google.com/earth/ (accessed on 30 May 2021).
44. Map Developers. Draw a circle—Create a Circle on a Google Map Using a Point and a Radius. 2021. Available online: https://www.mapdevelopers.com/draw-circle-tool.php (accessed on 30 May 2021).
45. Boeing, G. OSMnx: New methods for acquiring,constructing, analyzing, and visualizing complex street networks. *Comput. Environ. Urban Syst.* **2017**, *65*, 126–139. [CrossRef]
46. Aubé, M.; Marseille, C.; Farkouh, A.; Dufour, A.; Simoneau, A.; Zamorano, J.; Roby, J.; Tapia, C. Mapping the Melatonin Suppression, Star Light and Induced Photosynthesis Indices with the LANcube. *Remote Sens.* **2020**, *12*, 3954. [CrossRef]
47. Tscharntke, T.; Hochberg, M.E.; Rand, T.A.; Resh, V.H.; Krauss, J. Author sequence and credit for contributions in multiauthored publications. *PLoS Biol.* **2007**, *5*, e18. [CrossRef] [PubMed]